Table 1. *Clinical characteristics of patients with symptomatic peripheral artery disease and without peripheral artery disease (controls)*

	Disease control	Fontaine stage II PAD	Fontaine stage III PAD	Fontaine stage IV PAD	Total PAD	*P* value
No. of cases	92	46	20	70	136	—
Age, y, mean ± SD	69.3 ± 11.6	68.8 ± 7.1	74.5 ± 5.8	68.2 ± 9.8	69.3 ± 9.9	NS
Male (%)	62.0	91.3*	75.0	74.3	72.8†	*.001 vs control, †.003 vs control
Cardiovascular risk factors						
Hypertension (%)	80	63.0	95*	71.4	72.0	*.036 vs FII
Diabetes mellitus (%)	17	62.2*	47.4†	76.1*	65.0*	*<.001 vs control, †.026 vs control
Dyslipidemia (%)	44.7	21.7*	42.1	19.7†	22.8†	*.007 vs control, †<.001 vs control
Atrial fibrillation (%)	6.4	6.5	5.0	5.7	5.9	NS
Coronary artery disease (%)	14.9	41.3*	35.0	58.6†	49.3†	*.005 vs control, †<.001 vs control
Chronic kidney disease (%)	8.5	30.4*	35.0†	72.9‡	52.2‡	*.009 vs control, †.031 vs control, ‡≤.001 vs control/FII/FIII
Total cerebral infarctions (%)	29.0	47.8	85.0*†	68.6*	64.0*	*<.001 vs control, †.008 vs FII
Symptomatic infarction (%)	10.9	23.9	60.0*†	38.6*	36.8*	*<.001 vs control, †<.008 vs FII
Asymptomatic infarction (%)	18.5	23.9	25.0	30.0	27.2	NS
Total small infarctions (3-15 mm) (%)	23.9	39.1	55.0*	60.0†	52.2*	*.05 vs control, †<.001 vs control
Symptomatic (%)	4.3	15.2	25.0	32.9*	25.7*	*<.001 vs control
Asymptomatic (%)	19.6	23.9	30.0	27.1	26.5	NS
Total large infarctions (>15 mm) (%)	8.7	17.4	50.0*†	30.0‡	28.7*	*<.001 vs control, †.01 vs FII, ‡.004 vs control
Symptomatic (%)	7.6	15.2	45.0*†	27.1‡	25.7*	*<.001 vs control, †.02 vs FII, ‡.007 vs control
Asymptomatic (%)	1.1	2.2	5.0	2.9	2.9	NS
Cerebral hemorrhage (%)	5.3	4.4	10.0	8.6	7.4	NS
Fazekas score (mean ± SD)	1.8 ± 1.2	2.2 ± 1.0	2.8 ± 1.3*	2.8 ± 1.4†	2.6 ± 1.3†	*.008 vs control, †<.001 vs control
PVH score	1.1 ± 0.7	1.2 ± 0.5	1.5 ± 0.6	1.5 ± 0.7*†	1.4 ± 0.6‡	*<.001 vs control, †.01 vs FII, ‡.005 vs control
DWMH score	0.8 ± 1.2	1.1 ± 0.6*	1.3 ± 0.7†	1.3 ± 0.7‡	1.2 ± 0.7‡	*.02 vs control, †.007 vs control, ‡<.001 vs control
Supraclinoid ICA Stenosis >50% (%)	3.2	11.0	6.7	23.9*	17.3*	*≤.001 vs control

(Continued)

Table 1. Clinical characteristics of patients with symptomatic peripheral artery disease and without peripheral artery disease (controls) (*Continued*)

	Disease control	Fontaine stage II PAD	Fontaine stage III PAD	Fontaine stage IV PAD	Total PAD	*P* value
MCA (M1 portion)						
Stenosis >50% (%)	8.5	11.1	13.3	13.4	12.7	NS
Basilar artery						
Stenosis >50% (%)	0	0	0	6.0†	3.1	†.032 vs control
Cervical ICA						
Stenosis >50% (%)	2.5	23.8*	0	26.2†‡	21.8†	*.006 vs control, †<.001 vs control, ‡.032 vs FIII

Abbreviations: DWMH, deep white matter hyperintensity; FII, Fontaine stage II; FIII, Fontaine stage III; ICA, internal carotid artery; MCA, middle cerebral artery; NS, not significant; PVH, periventrocular hyperintensity; SD, standard deviation.

Post-hoc test (Bonferroni) was used for comparison between controls and each peripheral artery disease group. The Mann–Whitney *U* test was used for comparison between control and total PAD patients.

years) 8.1 (1.2-454.7), diabetes mellitus 12.4 (3.2-47.7), and CKD 30.1 (4.4-206.8). Many of the confidence intervals were very wide.

Discussion

Our study showed that 64% of the patients with PAD had symptomatic or asymptomatic cerebral infarctions, while only 29.0% of the controls did. Interestingly, there was no significant difference in the frequency of asymptomatic cerebral infarctions between each PAD group and the control group regardless of the infarction size. On the other hand, both symptomatic large and small infarctions were observed more frequently in the Fontaine III/IV PAD patients than in the controls. These results suggest that Fontaine III/IV PAD is closely associated with symptomatic cerebral infarction regardless of the lesion size, although the reason why only symptomatic cerebral infarction was frequently observed in PAD patients is unclear. Although there are few studies of the frequency of CVD in patients with symptomatic PAD, several studies reported the frequency of PAD diagnosed by ankle brachial index (ABI) assessment in patients with CVD and/or CAD. PAD is associated with a 6-fold increase in fatal and nonfatal MI,[6] and a 2- to 3-fold increase in the risk of incident ischemic CVD.[7] The Reduction of Atherothrombosis for Continued Health (REACH) Registry is an international prospective cohort of 68,236 patients with either established atherosclerotic arterial disease (CAD, PAD, and CVD; n = 55,814) or at least 3 risk factors for atherothrombosis (n = 12,422). In this large international study, the incidences of cardiovascular death, MI, stroke, or hospitalization for atherothrombotic event(s) increased with the number of symptomatic arterial disease locations, ranging from 12.58% for patients with 1, 21.14% for patients with 2, and 26.27% for patients with 3 symptomatic arterial disease locations ($P < .001$ for trend), suggesting that cardiovascular events including stroke are closely related with the progression of PAD.[8] Furthermore, in the Japanese population of the REACH registry, an ABI <0.9 was a significant predisposing factor for stroke and asymptomatic carotid stenosis ≥70%.[9]

Our data showed that the Fontaine III/IV PAD patients had WMLs more frequently than the control patients. The PVH score in only Fontaine stage IV PAD group was higher than that of the control group, while the DWMH score of all Fontaine stages of PAD groups was higher than that of the control group. These data suggest that DWMH is more closely associated with the symptomatic PAD than PVH. Our finding is consistent with the previous report that severe WML was significantly associated with PAD (hazard ratio 1.59, 95% CI 1.11-2.26; $P = .011$).[10] Cerebral white matter changes represent a vascular process linked mainly with cerebral small vessel changes,[11] indicating that Fontaine III/IV PAD patients

Table 2. *Multiple logistic regression analysis of patients with symptomatic peripheral artery disease and without peripheral artery disease (controls)*

	Disease control	Symptomatic PAD, OR (95% CI)	*P* value
Age >65 y	1.0	8.1 (1.2-454.7)*	.031
Male	1.0	3.1 (0.8-11.8)	.092
Cardiovascular risk factors			
Hypertension	1.0	0.2 (0-0.8)	.025
Diabetes mellitus	1.0	12.4 (3.2-47.7)*	<.001
Dyslipidemia	1.0	0.1 (0-0.4)	.001
Atrial fibrillation	1.0	4.1 (0.4-44.2)	.240
Coronary artery disease	1.0	3.4 (0.8-13.5)	.085
Chronic kidney disease	1.0	30.1 (4.4-206.8)*	<.001
Total cerebral infarctions	1.0	0.8 (0-34.6)	.902
Symptomatic infarction	1.0	1.5 (0-39.0)	.811
Total small infarctions (3-15 mm)	1.0	5.7 (0.1-264.5)	.372
Symptomatic	1.0	0.7 (0.1-9.4)	.681
Total large infarctions (>15 mm)	1.0	0.1 (0-1.2E + 30)	.921
Symptomatic	1.0	25.2 (0-1.2E + 33)	.931
Fazekas score >4	1.0	1854 (0-1.2E + 144)	.952
PVH score >2	1.0	1054 (0-7.0E + 142)	.966
DWMH score >2	1.0	6.3 (0-1.5E + 145)	.991
Supraclinoid ICA			
Stenosis >50% (%)	1.0	0.8 (0-9.8)	.860
MCA (M1 portion)			
Stenosis >50% (%)	1.0	0.2 (0-2.2)	.171
Basilar artery			
Stenosis >50% (%)	1.0	2568 (0-9.2E + 86)	.936
Cervical ICA			
Stenosis >50% (%)	1.0	1.3 (0.1-15.4)	.837

Abbreviations: CI, confidence interval; DWMH, deep white matter hyperintensity; ICA, internal carotid artery; MCA, middle cerebral artery; OR, odds ratio; PVH, periventrocular hyperintensity; SD, standard deviation.
*Significant odds ratio.

have cerebral small vessel changes in addition to symptomatic cerebral infarctions.

As far as we know, there is no report of a detailed MRA analysis of intracranial arteries in patients with symptomatic PAD. We evaluated intracranial artery stenosis using the criteria of the CATHARSIS study.[5] We found that supraclinoid ICA stenosis (>50%) was present in 23.9% of the Fontaine stage IV patients but present in only 3.2% of the control subjects. The frequency of supraclinoid ICA stenosis in Fontaine II and III patients was between those of control and Fontaine IV patients. There was no significant difference in the frequency of MCA stenosis (M1 portion) between the controls and PAD patients. In this study, we found a few significant basilar artery stenoses only in the Fontaine stage IV patients (6%). Although the degree of stenosis may be overestimated on MRA, supraclinoid ICA stenosis seems to be frequent in the Fontaine stage IV PAD patients.

There are many studies of stenosis of the cervical ICA in patients with PAD. An analysis of 5 studies indicated that 25% of PAD patients have significant stenosis of ICA.[3] In the study of a Chinese population, carotid stenosis ≥70% was found in 24.5% of patients with PAD, but in only 11.1% of patients with CAD,[12] indicating that PAD may be a stronger indicator of concomitant CVD than CAD in Asian populations. Cervical ICA stenosis was observed 21.8% of our PAD patients. Although the rate of stenosis may not be as accurate as those obtained with ultrasonography or 3-dimensional CT scan, the frequency of cervical ICA stenosis was similar to that in previous reports.

Hypertension and dyslipidemia are common risk factors for PAD,[13] but in this study hypertension (80%) and dyslipidemia (44.7%) showed little relationship to PAD. This may be in part because of the high prevalence of both hypertension and dyslipidemia in the control subjects. In contrast, diabetes mellitus seemed to be closely associated with all stages of PAD in this study. It has been reported that diabetes increases the risk of PAD by 3- to 4-fold over that of the general population.[14] Poor control of diabetes is also an independent risk factor for PAD: with every 1% increase in glycosylated hemoglobin, the risk of PAD has been shown to increase by 28%.[15] The frequency of CKD was higher in PAD patients of all stages (52.2%) than that in the controls (8.5%) in this study.

Multiple logistic regression analysis also showed a significantly high OR for CKD in PAD patients.

A potential limitation of our study is the possibility of selection bias: the Fontaine III patients had hypertension and dyslipidemia more frequently and diabetes mellitus less frequently than other PAD patients, probably partly because they were fewer in number and slightly older. Another limitation of our study is the lack of data on cigarette smoking as an important risk factor for PAD. The wide range of CIs in the multiple logistic regression analysis requires additional study to validate our results. Again, the stenosis of an artery is usually overestimated using MRA. These may limit generalization of the results. Despite of these limitations, our study provides a new insight into the relationship between cerebral infarction, cerebral WML, and intracranial artery disease as well as extracranial artery disease in patients with symptomatic PAD.

In conclusion, advanced PAD patients have an increased prevalence of symptomatic cerebral infarction, WML, and intracranial ICA stenosis as well as diabetes mellitus, CAD, CKD, and cervical ICA stenosis.

References

1. Poredos P, Jug B. The prevalence of peripheral arterial disease in high risk subjects and coronary or cerebrovascular patients. Angiology 2007;58:309-315.
2. Heald CL, Fowkes FG, Murray GD, et al. Risk of mortality and cardiovascular disease associated with the ankle-brachial index: Systematic review. Atherosclerosis 2006; 189:61-69.
3. Golomb BA, Dang TT, Criqui MH. Peripheral arterial disease: Morbidity and mortality implications. Circulation 2006;114:688-699.
4. Fazekas F, Chawluk JB, Alavi A, et al. MR signal abnormalities at 1.5T in Alzheimer's dementia and normal aging. Am J Neuroradiol 1987;8:421-426.
5. Uchiyama S, Sakai N, Kimura Y, et al. Cilostazol-aspirin therapy against recurrent stroke with intracranial artery stenosis (CATHARSIS). ClinicalTrials.gov Identifier: NCT00333164, 2006.
6. Criqui MH, Langer RD, Fronek A, et al. Mortality over a period of 10 years in patients with peripheral arterial disease. N Engl J Med 1992;326:381-386.
7. Zheng ZJ, Sharrett AR, Chambless LE, et al. Associations of ankle brachial index with clinical coronary heart disease, stroke and preclinical carotid and popliteal atherosclerosis: The Atherosclerosis Risk in Communities (ARIC) Study. Atherosclerosis 1997; 131:115-125.
8. Steg PG, Bhatt DL, Wilson PW, et al. One-year cardiovascular event rates in outpatients with atherothrombosis. JAMA 2007;297:1197-1206.
9. Uchiyama S, Goto S, Matsumoto M, et al. Cardiovascular event rates in patients with cerebrovascular disease and atherothrombosis at other vascular locations: Results from 1-year outcomes in the Japanese REACH Registry. J Neurol Sci 2009;287:45-51.
10. Oksala NK, Oksala A, Pohjasvaara T, et al. Age related white matter changes predict stroke death in long term follow-up. J Neurol Neurosurg Psychiatry 2009; 80:762-766.
11. Pantoni L, Garcia JH. Pathogenesis of leukoaraiosis: A review. Stroke 1997;28:652-659.
12. Cheng SW, Wu LL, Lau H, et al. Prevalence of significant carotid stenosis in Chinese patients with peripheral and coronary artery disease. Aust NZ J Surg 1999; 69:44-47.
13. Stoyioglou A, Jaff MR. Medical treatment of peripheral arterial disease: A comprehensive review. J Vasc Interv Radiol 2004;15. 1197-1207.
14. Kannel WB, Skinner J Jr, Schwartz MJ, et al. Intermittent claudication. Incidence in the Framingham Study. Circulation 1970;41:875-883.
15. Selvin E, Marinopoulos S, Berkenblit G, et al. Meta-analysis: Glycosylated hemoglobin and cardiovascular disease in diabetes mellitus. Ann Intern Med 2004; 141:421-431.

Supplemental Material can be found at:
http://www.jbc.org/content/suppl/2011/10/25/M111.284729.DC1.html

THE JOURNAL OF BIOLOGICAL CHEMISTRY VOL. 286, NO. 50, pp. 43549–43558, December 16, 2011
© 2011 by The American Society for Biochemistry and Molecular Biology, Inc. Printed in the U.S.A.

Compensatory Regulation of Dopamine after Ablation of the Tyrosine Hydroxylase Gene in the Nigrostriatal Projection*[S]

Received for publication, July 20, 2011, and in revised form, October 6, 2011 Published, JBC Papers in Press, October 25, 2011, DOI 10.1074/jbc.M111.284729

Hirofumi Tokuoka[‡1], Shin-ichi Muramatsu[§], Chiho Sumi-Ichinose[¶], Hiroaki Sakane[‡], Masayo Kojima[‡], Yoshinori Aso[‡], Takahide Nomura[¶], Daniel Metzger[‖‡‡], and Hiroshi Ichinose[‡2]**

*From the [‡]Department of Life Science, Graduate School of Bioscience and Biotechnology, Tokyo Institute of Technology, 4259 B-7, Nagatsuta, Midori-ku, Yokohama, 226-8501 Japan, the [§]Division of Neurology, Department of Medicine, Jichi Medical University, Tochigi 329-0498, Japan, the [¶]Department of Pharmacology, School of Medicine, Fujita Health University, Toyoake, Aichi 470-1192, Japan, the [‖]Institut de Génétique et de Biologie Moléculaire et Cellulaire, Illkirch F-67400, France, **CNRS, Illkirch, France, and the [‡‡]Université Louis Pasteur, Strasbourg F-67000, France*

Background: The tyrosine hydroxylase (TH) gene, essential for dopamine synthesis, is partially ablated in adult nigrostriatal projection.
Results: TH reduction in axon terminals is slower than in soma, and dopamine is better maintained than TH.
Conclusion: Striatal dopamine is compensatorily regulated by axonal TH level and L-DOPA synthesis activity per TH level.
Significance: This regulation has potential relevance to pathogenesis of Parkinson disease and other dopamine-related psychiatric disorders.

The tyrosine hydroxylase (TH; EC 1.14.16.2) is a rate-limiting enzyme in the dopamine synthesis and important for the central dopaminergic system, which controls voluntary movements and reward-dependent behaviors. Here, to further explore the regulatory mechanism of dopamine levels by TH in adult mouse brains, we employed a genetic method to inactivate the *Th* gene in the nigrostriatal projection using the Cre-*loxP* system. Stereotaxic injection of adeno-associated virus expressing Cre recombinase (AAV-Cre) into the substantia nigra pars compacta (SNc), where dopaminergic cell bodies locate, specifically inactivated the *Th* gene. Whereas the number of TH-expressing cells decreased to less than 40% in the SNc 2 weeks after the AAV-Cre injection, the striatal TH protein level decreased to 75%, 50%, and 39% at 2, 4, and 8 weeks, respectively, after the injection. Thus, unexpectedly, the reduction of TH protein in the striatum, where SNc dopaminergic axons innervate densely, was slower than in the SNc. Moreover, despite the essential requirement of TH for dopamine synthesis, the striatal dopamine contents were only moderately decreased, to 70% even 8 weeks after AAV-Cre injection. Concurrently, *in vivo* synthesis activity of L-dihydroxyphenylalanine, the dopamine precursor, per TH protein level was augmented, suggesting up-regulation of dopamine synthesis activity in the intact nigrostriatal axons. Collectively, our conditional *Th* gene targeting method demonstrates two regulatory mechanisms of TH in axon terminals for dopamine homeostasis *in vivo*: local regulation of TH protein amount independent of soma and trans-axonal regulation of apparent L-dihydroxyphenylalanine synthesis activity per TH protein.

The dopaminergic system is important for many brain functions, including voluntary movements (1) and reward-related behaviors (2). The dysfunction of dopaminergic transmission is involved in many neurological and psychiatric disorders, such as Parkinson disease (3), addiction (4), attention deficit hyperactive disorders (5), and schizophrenia (6). Although chronic alterations in the dopaminergic system may be relevant to these disorders, it is still unclear how the dopaminergic system is regulated over days to months. In Parkinson disease, motor symptoms exhibit only after a large loss of striatal dopamine (7), suggesting compensation for the loss of dopamine. Although studies on Parkinson disease have suggested multiple forms of compensatory mechanisms, including enhanced dopamine release and turnover (8, 9, 10, 11), it is not fully understood what cellular and molecular mechanisms underlie the long term regulation of striatal dopamine levels under non-degenerative conditions.

Chronic intervention in the dopamine system has been performed for many years by pharmacological methods although they exhibit limitations related to dose dependence, drug metabolism, and circuit specificity. Gene-targeting methods, including germ line knock-out mice (12–14) and dopamine-deficient mice (15–17), have been generated, but because dopaminergic transmissions are blocked from the early stage of brain development, these methods may induce developmental effects. To explore the regulatory mechanisms of the nigrostriatal dopaminergic system in the adult brain, we generated mice in which dopamine synthesis can be selectively abrogated in a spatio-temporally controlled manner. The nigrostriatal projection is the largest dopaminergic projection in the brain, and the dense dopaminergic axon terminals in the striatum are readily

* This work was supported by Grants-in-aid for Human Frontier Science Program; by Research Grant 18A-2 for Nervous and Mental Disorders from the Ministry of Health, Labor and Welfare of Japan; by KAKENHI from MEXT; by the Nakajima Foundation; and by Core Research for Evolutional Science and Technology, Japan Science and Technology Agency (CREST, JST).
[S] The on-line version of this article (available at http://www.jbc.org) contains supplemental Figs. 1–5.
[1] To whom correspondence may be addressed. Tel.: 81-45-924-5822; Fax: 81-45-924-5807; E-mail: htokuoka@bio.titech.ac.jp.
[2] To whom correspondence may be addressed. Tel.: 81-45-924-5822; Fax: 81-45-924-5807; E-mail: hichinos@bio.titech.ac.jp.

Downloaded from www.jbc.org at JICHI IKA DAIGAKU, on February 27, 2012

investigated in isolation from their cell bodies and dendrites. Because tyrosine hydroxylase (TH)[3] is the rate-limiting enzyme in dopamine biosynthesis (18), we generated transgenic mice that contain two *loxP* sites flanking the major coding exons of the *TH* gene (floxed *Th* mice).

A microinjection of adeno-associated viral (AAV) vector expressing Cre recombinase (AAV-Cre) (19, 20) into the substantia nigra pars compacta (SNc) of the floxed *Th* mice disrupted the expression of the *Th* gene in a subset of neurons in the SNc of the adult mice. Our biochemical and histochemical analyses suggest two regulatory mechanisms of axonal TH for dopamine homeostasis in the nigrostriatal projection. First, the TH protein level in axon terminals is regulated differently from that in soma. Second, *in vivo* apparent L-DOPA synthesis activity per TH protein level in a given axon is influenced by dopamine synthesis in the neighboring axons, which we propose as trans-axonal regulation of dopamine levels.

EXPERIMENTAL PROCEDURES

Production of Th Floxed Mice, Genotyping—To construct the targeting vector for generating a floxed *Th* allele, a 9.5-kb XhoI-EcoRI genomic DNA segment containing genomic *Th* DNA was isolated from a λ phage 129SV mouse genomic library. The EcoRI site located at the 3′-end was replaced by MluI, a HindIII restriction site was engineered by site-directed mutagenesis between exons 5 and 6, and the SpeI site located between exons 9 and 10 was converted into a NotI site. A *loxP* site and an EcoRV restriction site were inserted into a HindIII site, and a neomycin-resistant cassette, flanked by *loxP* sites, was inserted into a NotI site. The three *loxP* sites in the final targeting vector were in the same orientation (3′ to 5′) (Fig. 1*A*).

Mouse embryonic stem cells were electroporated with the targeting vector, and the homologously recombinated clones were screened by PCR and Southern blot analysis. Embryonic stem clones with three *loxP* sites were selected, and a plasmid expressing Cre DNA recombinase was transiently transfected into the cells. Embryonic stem cells with two *loxP* sites without a neomycin cassette were selected by PCR and used for production of chimeric mice.

The genotypes of mice were identified on mouse ear biopsies by PCR (30 cycles at 94 °C for 30 s, 65 °C for 3 min, and a final extension at 72 °C for 5 min) with primers TH9F (5′-CATTTGCCCAGTTCTCCCAG-3′) and TH10R (5′-AGAGATGCAAGTCCAATGTC-3′). The sizes of the PCR products amplified from the wild-type *Th* allele and from the floxed *Th* allele are 431 and 513 bp, respectively.

For the detection of recombined *Th* alleles, genomic DNA was extracted from the substantia nigra regions of brain slices fixed by paraformaldehyde. The recombined *Th* alleles were detected by PCR (30 cycles at 94 °C for 30 s, 66 °C for 30 s, 72 °C for 1 min 15 s, and a final extension at 72 °C for 5 min) with primers TH5F (5′-AGGCGTATCGCCAGCGCC-3′) and TH10Rb (5′-CCCCAGAGATGCAAGTCCAATGTC-3′). The sizes of the PCR products amplified from the wild-type *Th* allele, floxed *Th* allele, and deleted *Th* allele are 1722, 1886, and 430 bp, respectively.

AAV Vector Construction—We generated two types of AAV-Cre vectors basically as described previously (19). One was the AAV-Cre vector, which contained an expression cassette with a human cytomegalovirus immediate early promoter (CMV promoter), followed by the first intron of human growth hormone, Cre recombinase cDNA, and simian virus 40 polyadenylation signal sequence (SV40 poly(A)), between the inverted terminal repeats of the AAV-2 genome. The other was the AAV-GFP/Cre vector, which contained an expression cassette with a synapsin I promoter (21), followed by AcGFP1 (Clontech), the internal ribosomal entry site, Cre recombinase cDNA, and simian virus 40 polyadenylation signal sequence (SV40 poly(A)), between the inverted terminal repeats of the AAV-1 genome. The two helper plasmids, pHLP19 and pladeno1 (Avigen, Alameda, CA), harbored the AAV *rep* and *cap* genes as well as the E2A, E4, and VA RNA genes of the adenovirus genome, respectively. HEK293 cells were co-transfected with the vector plasmid, pHLP19, and pladeno1 by the calcium phosphate precipitation method. The AAV vectors were then harvested and purified by two rounds of continuous iodoxale ultracentrifugations. Vector titers were determined by quantitative DNA dot-blot hybridization or by quantitative PCR of DNase I-treated vector stocks. We routinely obtained 10^{12} to 10^{13} vector genome copies/ml.

Animals and Stereotaxic Microinjections—Mice were acclimated to and maintained at 25 °C under a 12-h light/dark cycle (light on 08:00–20:00). All animal experiments were performed in accordance with the general guidelines of the Tokyo Institute of Technology. Unilateral injections into the SNc were performed on 12–16-week-old mice that were anesthetized with Nembutal (intraperitoneally) and mounted into a stereotaxic apparatus. The coordinates were 3.0 mm posterior from bregma, 1.0 mm lateral to midline, and 4.0 mm ventral from the dural surface. 1 μl of AAV-Cre or AAV-GFP/Cre (about 10^9 particles) was injected through an injection cannula (28-gauge) with a Hamilton microsyringe driven by a microdialysis pump at a rate of 0.2 μl/min. After microinjection, the injection cannula was left for 2 min before its withdrawal to reduce the efflux of injected liquid along the injection tract. When a cannula was blocked or leaked, the mouse was excluded from the following experiments. The mice were sacrificed at 1, 2, 4, 8, or 16 weeks after microinjection for analyses. We used the uninjected side of a brain as a control side to compare with. $Th^{+/+}$ mice were used as control animals.

Immunohistochemistry—Striatal slices were prepared by transcardial perfusion with saline, followed by 4% paraformaldehyde, 60 mM phosphate buffer, and postfixation overnight. All solutions were used at 4 °C. In some experiments, striatal tissues were dissected and homogenized for Western blot and monoamine assay (see below), and the rest of the brain, including the midbrain with the SNc region, was fixed by immersing in 4% paraformaldehyde, PBS overnight. The fixed brain pieces

[3] The abbreviations used are: TH, tyrosine hydroxylase; AADC, aromatic L-amino acid decarboxylase; AAV, adeno-associated virus; AAV-Cre, adeno-associated virus expressing Cre recombinase; DA, dopamine; DAT, dopamine transporter; DOPAC, 3,4-dihydroxyphenylacetic acid; HVA, homovanillic acid; L-DOPA, L-dihydroxyphenylalanine; vMAT2, vesicular monoamine transporter 2; SNc, substantia nigra pars compacta; 6-OHDA, 6-hydroxydopamine; GBR12909, 1-[2-[bis-(4-fluorophenyl)methoxy]ethyl]-4-(3-phenylpropyl)piperazine dihydrochloride.

Downloaded from www.jbc.org at JICHI IKA DAIGAKU, on February 27, 2012

were cryoprotected by 30% sucrose, and the coronal slices of 30-μm thickness were cut by a cryostat. The free floating serial coronal sections, from the rostral to the caudal edge of SNc or a part of the striatum, were incubated with rabbit anti-TH antibody (1:10,000; Millipore) or rabbit anti-AADC serum (1:20,000) (12), followed by biotinylated goat anti-rabbit IgG antibody (1:250; Vector Laboratories) and avidin-peroxidase complex (Vectastain ABC kit, Vector Laboratories). Immunocomplexes were visualized by a reaction with 3,3′-diaminobenzidine tetrahydrochloride and 0.003% H_2O_2. Images were taken using an upright microscope (Eclipse E800, Nikon) equipped with a cooled CCD camera (VB-6010, Keyence).

The numbers of TH-positive neurons in the injected and uninjected side SNc were compared using a stereological cell counting method. SNc was defined according to the brain atlas (22). Briefly, one in every three coronal sections covering the whole SNc was selected (typically 12–14 sections) and stained for TH, and magnified images of SNc were taken using a 20× objective lens (numerical aperture 0.5). For each region of interest, images were taken at multiple different focus planes to visualize all cells in the thickness. The number of all TH-positive cells in SNc in each slice was counted manually with ImageJ (National Institutes of Health). Only cells with an apparently visible nucleus were included. The number of all TH-positive neurons from a set of slices was summed (typically 1600–2000 cells in the uninjected side), and the ratio of the number in the injected side to that in the uninjected side was evaluated.

For fluorescence immunohistochemistry, the following secondary antibodies were used: Alexa546-conjugated anti-mouse IgG (1:2,000; Invitrogen) and Alexa633-conjugated anti-rabbit IgG (1:2,000; Invitrogen). Images were taken using the TCS SPE confocal microscope (Leica) with a 63× oil objective lens and excitation lasers of 532 and 635 nm.

For the detection of dopamine, we fixed mice transcardially with 5% glutaraldehyde, and the brain sections made with vibratome were stained with rabbit anti-TH antibody or rabbit anti-dopamine-glutaraldehyde conjugate (1:500; Millipore). Because glutaraldehyde fixation induces very strong background fluorescence, we performed immunodetection with the avidin-peroxidase complex as described above instead of fluorescence detection.

Western Blotting—To dissect striatal tissues for biochemical assays, we first made a coronal section of 2-mm thickness from approximately +1.5 to 0.5 mm to the bregma using a brain matrix (Neuroscience, Inc., Tokyo). Then the left and right dorsal striata were dissected by a surgical blade under a stereo microscope and homogenized using the Pellet Mixer (TreffLab) in 150 μl of PBS containing 1 mM dithiothreitol, 2 mM EDTA, 2 mM NaF, 1 μg/ml leupeptin, 1 μg/ml pepstatin, 1 mM phenylmethylsulfonyl fluoride, and 0.1 mM pargyline, followed by centrifugation at 20,000 × *g* for 10 min at 4 °C. An aliquot of the supernatant was used for the monoamine assay. In some experiments, ventral midbrain homogenates were prepared similarly, except the positions of coronal sections were approximately −2.5 to −4.5 mm to the bregma. The striatal or ventral midbrain homogenates containing 10 μg of protein were separated by electrophoresis on a 10% SDS-polyacrylamide gel and transferred to a PVDF membrane. The membranes were immunodetected using the following primary antibodies: rabbit anti-TH antibody (1:10,000; Millipore), rabbit anti-AADC antibody (1:20,000) (12), or mouse anti-β-actin antibody (1:10,000; Sigma-Aldrich). Immunoreactive proteins were detected by peroxidase-conjugated secondary antibodies and Immobilon-Western (Millipore). Quantitative analyses were performed with LAS-3000 (Fujifilm).

For better quantification of low level TH proteins by Western blot, we assessed the linearity of the detection using serial dilution of striatal homogenates of the uninjected side (supplemental Fig. 1). Then we employed a range showing a linear relationship between actual loaded proteins (2.5–20 μg, or a 0.125–1.0 ratio) and measured TH protein levels (0.05–1 ratio). Within this range, we made a standard curve and calibrated the TH protein levels accordingly.

For detection of vesicular monoamine transporter 2 (vMAT2) and dopamine transporter (DAT) proteins, a crude synaptosomal fraction was prepared by homogenizing striatal tissues in 4 mM HEPES buffer containing 0.32 M sucrose, 2 mM NaF, 1 μg/ml leupeptin, 1 μg/ml pepstatin, 1 mM phenylmethylsulfonyl fluoride, and 0.1 mM pargyline. The homogenate was centrifuged at 900 × *g*, the supernatant was further centrifuged at 14,500 × *g*, and the resulting pellet (P2 fraction) was dissolved in 80 μl of the same HEPES buffer containing 1% SDS. Protein concentration was determined by the DC protein assay (Bio-Rad). 20 μg of each protein sample was analyzed by Western blot using the following primary antibodies: rabbit anti-vMAT2 antiserum (1:500; Synaptic Systems), rabbit anti-DAT antibody (1:500; Millipore), rabbit anti-TH antibody (1:10,000; Millipore), or mouse anti-β-actin antibody (1:10,000; Sigma-Aldrich).

For the detection of phospho-TH proteins, striatal homogenates were prepared by immediate boiling of a whole brain for 5 min after dissection, followed by isolation of striata and homogenization and sonication in 0.1 M Tris-HCl (pH 6.8) buffer containing 1% SDS. Protein concentration was determined by the DC protein assay (Bio-Rad). 60 μg of each protein sample was analyzed by Western blot using the following primary antibodies: rabbit anti-Ser(P)-40-TH antibody (1:2,000; Millipore), rabbit anti-p31-TH antibody (1:2,000; Millipore), or rabbit anti-TH antibody (1:10,000; Millipore).

Monoamine Assay—Aliquots of striatal supernatant were deproteinized by 60 mM perchloric acid with 30 μM EDTA and 30 μM pargyline on ice for 30 min and centrifuged at 20,000 × *g* for 15 min. The monoamine levels in the supernatant were analyzed by high performance liquid chromatography (HPLC) with an SC5-ODS column (EICOM) and a mobile phase buffer containing 84 mM acetic acid-citrate (pH 3.5), 5 μg/ml EDTA, 190 mg/ml sodium 1-octane sulfonate, and 16% methanol. Monoamines were detected by electrochemical detection (ECD-100, EICOM).

Biopterin contents were measured as described previously (43). Briefly, the deproteinized homogenates were oxidized by 0.1 M HCl containing 0.1% I_2 and 0.2% KI for 1 h at room temperature, followed by centrifugation at 20,000 × *g* for 10 min. The supernatants were neutralized by 0.2% ascorbic acid and then subjected to HPLC analyses with Inertsil ODS-3 column (GL Sciences) and a mobile phase buffer containing 10 mM

Downloaded from www.jbc.org at JICHI IKA DAIGAKU, on February 27, 2012

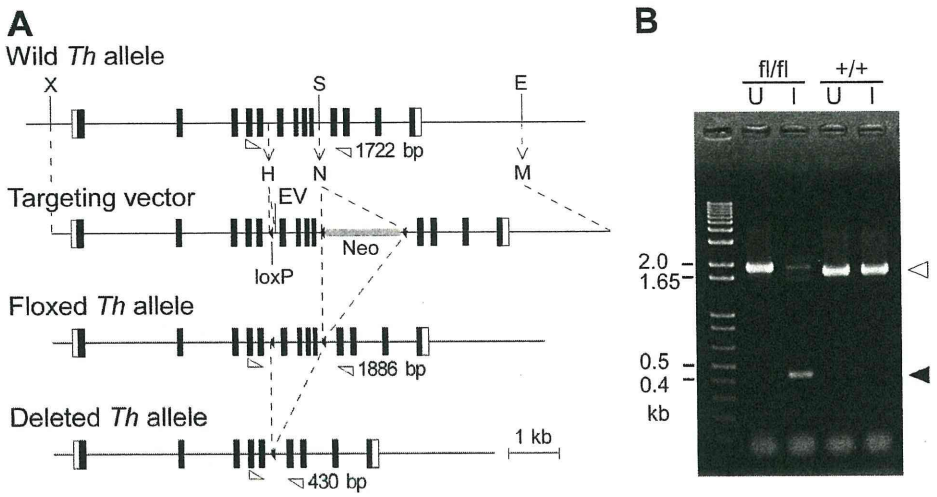

FIGURE 1. **Ablation of the *Th* gene by AAV-Cre injection into the SNc of the floxed *Th* mice.** *A*, schematic representation of the targeting vector for the generation of the floxed *Th* allele. *E*, EcoRI; *H*, HindIII; *M*, MluI; *N*, NotI; *S*, SpeI; *X*, XhoI; *Neo*, neomycin-resistant cassette. *Broken arrows* represent the generation or replacement of a restriction site. Exons are represented by *boxes*. The positions of the primers designed for the detection of genomic DNA recombination by PCR are indicated by *open triangles* with resulting PCR product sizes. *B*, PCR detection of genomic DNA recombination using primers for wild type (*open arrowhead*) or deleted *Th* (*closed arrowhead*) alleles. The template genomic DNA was prepared from the uninjected (*U*) or injected (*I*) side of the of the $Th^{fl/fl}$ or $Th^{+/+}$ mice 2 weeks after the unilateral microinjection of the AAV-Cre into the SNc. Note that the *Th* gene recombination was detected only in the injected side of the SNc of the $Th^{fl/fl}$ mice but not in the uninjected side of the $Th^{fl/fl}$ mice and the $Th^{+/+}$ mice.

$NaPO_4$ (pH 6.9) and a fluorescence detector (excitation 350 nm/emission 440 nm; RF-10A, Shimadzu, Tokyo).

Estimation of in Vivo L-DOPA Synthesis Activity per TH Protein Level—In vivo L-DOPA synthesis activity was evaluated by measuring the L-DOPA levels that accumulated in 30 min after the administration of 3-hydroxybenzylhydrazine dihydrochloride (NSD-1015, Sigma-Aldrich), an AADC inhibitor, to mice (100 mg/kg, intraperitoneal). The striatal tissues were homogenized using a pellet mixer (TreffLab) in 150 μl of PBS containing 1 mM dithiothreitol, 2 mM EDTA, 2 mM NaF, 1 μg/ml leupeptin, 1 μg/ml pepstatin, 1 mM phenylmethylsulfonyl fluoride, and 0.1 mM pargyline, followed by centrifugation at 20,000 $\times$ *g* for 10 min at 4 °C. An aliquot of the supernatant was used for assaying protein concentration by Bradford method, and Western blot to assess the TH protein levels. Another aliquot was deproteinized by 60 mM perchloric acid with 30 μM EDTA and 30 μM pargyline on ice for 30 min and centrifuged at 20,000 $\times$ *g* for 15 min. The supernatant was neutralized by K_2CO_3, and L-DOPA was purified by Al_2O_3 powder. The L-DOPA level was analyzed by HPLC with a NUCLEOSIL 100-7C18 reverse-phase column with a mobile phase buffer containing 0.1 M $NaPO_4$ (pH 3.5), 8 μM EDTA and electrochemical detection. To evaluate the *in vivo* L-DOPA synthesis activity per TH protein, L-DOPA accumulation was normalized to TH protein levels estimated by Western blot.

Rotation Test—Mice were placed in a round bowl (25 cm in diameter) for 20 min for acclimation. The mice were administered with 1-[2-[bis-(4-fluorophenyl)methoxy]ethyl]-4-(3-phenylpropyl)piperazine dihydrochloride (GBR12909; Tocris Bioscience; intraperitoneal, 30 mg/kg) and returned to the same bowl, and the behavior was videorecorded. The rotations were counted by visual observation for a 60-min period immediately after intraperitoneal injection. One rotation was defined by the animal completing a 360° turning without turning back in the opposite direction.

Statistics—The Mann-Whitney *U* test, Wilcoxon's signed rank test, or Steel's test was used as required. Spearman's rank correlation was used to evaluate a correlation between two groups. p values of <0.05 were considered significant. The data are shown as individual data points and mean values or as mean ± S.E., as indicated. Exponential and liner fittings were performed with Igor Pro 6.2 (WaveMetrics).

RESULTS

Production of Floxed Th Mice and Th Gene Ablation by AAV-Cre—First, we generated the floxed *Th* mice ($Th^{fl/fl}$) in which exons 6–9 of the *Th* gene were flanked by *loxP* sites (Fig. 1*A*). We used AAV-Cre to induce DNA recombination *in vivo* by performing a unilateral stereotaxic microinjection of the virus into the SNc of the adult floxed *Th* mice. Microinjection of AAV-Cre into the SNc induced DNA recombination in 2 weeks when we examined the substantia nigra tissue samples by PCR (Fig. 1*B*). *Th* gene recombination was detected in the injected side SNc of the $Th^{fl/fl}$ mice but not in the uninjected side of the $Th^{fl/fl}$ mice and both sides of the $Th^{+/+}$ mice. Thus, the floxed *Th* mice and AAV-Cre enabled us to induce *Th* gene ablation in the adult mouse midbrain.

Abrogation of TH Protein Expression in SNc Dopaminergic Neurons—Using immunohistochemistry, we next examined the effect of the AAV-Cre injection on TH protein expression in the SNc. The TH protein immunoreactivity was absent in the majority of neurons in the SNc 2 weeks after the AAV-Cre injection (Fig. 2*A* and *B*). We found that the number of TH-positive dopaminergic neurons normalized to the uninjected side was reduced by as early as 2 weeks, with the mean ratios of 38, 30, and 40% at 2, 4, and 8 weeks after the AAV-Cre injection, respectively, whereas they were unchanged in the $Th^{+/+}$ mice (97% at 8 weeks; Steel's test, $p = 0.0239$, 0.0166, and 0.0061 for the $Th^{fl/fl}$ mice at 2, 4, and 8 weeks, respectively, compared with the $Th^{+/+}$ at 8 weeks; Fig. 2*C*).

Downloaded from www.jbc.org at JICHI IKA DAIGAKU, on February 27, 2012

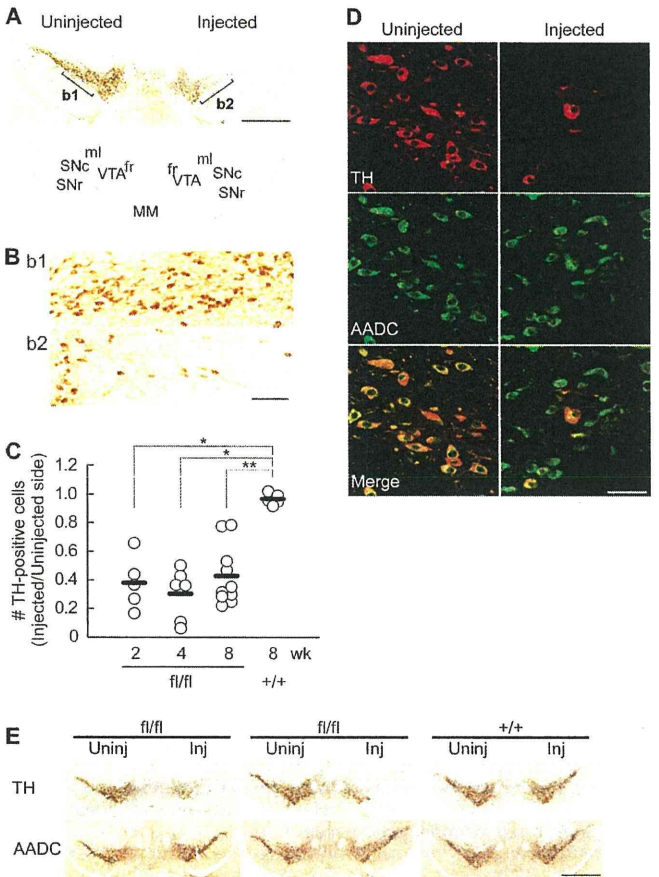

FIGURE 2. **AAV-Cre-induced loss of TH expression in the SNc.** *A*, a representative image of a midbrain slice immunostained for TH (*top*) and a schematic atlas (*bottom*). Serial coronal sections of the midbrains of the $Th^{fl/fl}$ mice were prepared 8 weeks after the AAV-Cre injection and were immunostained for TH. The SNc in the atlas is indicated by the *hatched area*. *fr*, fasciculus retroflexus; *ml*, medial lemniscus; *MM*, medial mammillary nucleus; *SNr*, substantia nigra pars reticulata; *VTA*, ventral tegmental area. *B*, magnified views of the uninjected side (*b1*) and injected side (*b2*) SNc as indicated in *A*. *C*, summary of the ratio of TH-positive cell numbers in the injected side SNc to the uninjected side. *Open circles* indicate the values from individual animals, and *bars* indicate the means. $n = 5$, 6, 11, and 5 brains for 2, 4, and 8 weeks ($Th^{fl/fl}$ mice) and 8 weeks ($Th^{-/-}$ mice) after injection, respectively. *, $p < 0.05$; **, $p < 0.01$, Steel's test. *D*, immunofluorescence staining for TH (*red*) and AADC (*green*) of the SNc of the $Th^{fl/fl}$ mice examined 2 weeks after the injection of AAV-GFP/Cre. TH and AADC were visualized with Alexa546 and Alexa633, respectively, distinguishing from GFP signal, and *pseudocolored* confocal images are shown. Note that the number of TH-expressing neurons was clearly reduced in the AAV-GFP/Cre-injected side, whereas the AADC, another dopaminergic neuron marker, remained expressed. *E*, TH deletion induces no apparent cell death in 16 weeks. Midbrain slices from two $Th^{fl/fl}$ mice and one $Th^{+/+}$ mouse were immunostained for TH and AADC 16 weeks after the AAV-Cre microinjection. Whereas the TH-expressing neurons were reduced in the injected side of the SNc of the $Th^{fl/fl}$ mice, the number of AADC-expressing neurons was apparently unaffected, suggesting that the dopaminergic neurons do not show cell death in the absence of TH in 16 weeks. *Scale bars*, 1 mm (*A*), 100 μm (*B*), 50 μm (*D*), and 1 mm (*E*).

To confirm a selective loss of TH protein, we also performed double immunofluorescence histochemistry for TH and aromatic AADC, a dopaminergic neuron marker. We used AAV-GFP/Cre for the purpose of labeling infected cells, but GFP expression in these neurons was too weak for detection, so we immunostained TH and AADC with Alexa546 and Alexa633 fluorophores, respectively, distinguishing from GFP signals. We found that the AADC immunoreactivity was preserved in the TH-negative neurons in the SNc 2 weeks after the AAV-GFP/Cre injection (Fig. 2*D*), suggesting that the AAV-GFP/Cre injection induced an efficient *Th* gene ablation without inducing cell death or damage. Moreover, AADC expression in the SNc was apparently unaffected in the $Th^{fl/fl}$ mice up to 16 weeks following the AAV-Cre injection, when the majority of the SNc dopaminergic neurons lost TH expression (Fig. 2*E*). These data suggest that dopamine is not essential for the survival of dopaminergic neurons in adult brains.

Slower Reduction of TH Proteins in Axon Terminals of Nigrostriatal Projection—The dopaminergic neurons in the SNc project their axons toward the striatum and form dense synapses (23, 24), where abundant TH proteins were contained. We quantitatively examined the reduction of the TH protein in the striatum by Western blot (Fig. 3*A* and *B*). The TH protein level was gradually reduced in the AAV-Cre injected side compared with the uninjected side in $Th^{fl/fl}$ mice, to 75, 50, and 39% at 2, 4, and 8 weeks after the AAV-Cre injection, respectively, whereas the levels were unchanged in the $Th^{+/+}$ mice (104% at 8 weeks; Steel's test, $p = 0.0932$, 0.0071, and 0.0059 for the $Th^{fl/fl}$ mice at 2, 4, and 8 weeks, respectively, compared with the $Th^{-/-}$ at 8 weeks; Fig. 3*B*). AADC protein levels did not show significant changes (Steel's test, $p = 0.77$, 0.92, and 0.88 for the $Th^{fl/fl}$ mice at 2, 4, and 8 weeks, respectively, compared with the $Th^{+/+}$ at 8 weeks; supplemental Fig. 2*A*).

We noticed that the reduction of TH protein level in the striatum could be slower than the reduction of the number of TH-expressing cells in the SNc because the difference between the two seemed remarkable at 2 weeks. To further investigate the difference, we compared the TH protein reductions in the striatum with that in ventral midbrain tissue, including SNc, using Western blot (Fig. 3*C*). We found that the TH protein reduction in the striatum showed a delay by about 2 weeks, whereas the decay time constants were similar ($\tau = 2.06$ and 2.04 weeks for the ventral midbrain and striatum, respectively).

We also used immunofluorescence histochemistry to examine the expression of TH and AADC in the striatum (Fig. 3*D*). Two weeks after the AAV-Cre injection, the number of TH-expressing axons in the injected side of the striatum of the $Th^{fl/fl}$ mice was only slightly reduced compared with the uninjected side, which was consistent with the Western blot data. However, the number of TH-expressing axons was decreased profoundly 8 weeks after the AAV-Cre injection. The number of AADC-expressing axons was apparently unchanged, suggesting that the axon terminals of the dopaminergic neurons remained mostly intact. These Western blot and immunohistochemical data indicate differential regulation of TH protein levels between axon terminals (striatum) and soma (SNc). Also, the *Th* gene ablation led to an almost complete and selective loss of TH protein in a subset of dopaminergic axons.

Better Maintenance of Striatal Dopamine Levels than TH Protein Levels—To investigate if dopamine levels follow the reduction of TH protein levels in the striatum, we assayed striatal monoamine contents using the same striatal extracts used in the Western blot analysis (Fig. 4*A*). The dopamine contents decreased gradually to around 98, 79, and 69% at 2, 4, and 8 weeks after the AAV-Cre injection, respectively, in the $Th^{fl/fl}$ mice but not in the $Th^{+/+}$ mice (104% at 8 weeks; Steel's test, $p = 0.98$, 0.0475, and 0.0637 for 2, 4, and 8 weeks in the $Th^{fl/fl}$

Downloaded from www.jbc.org at JICHI IKA DAIGAKU, on February 27, 2012

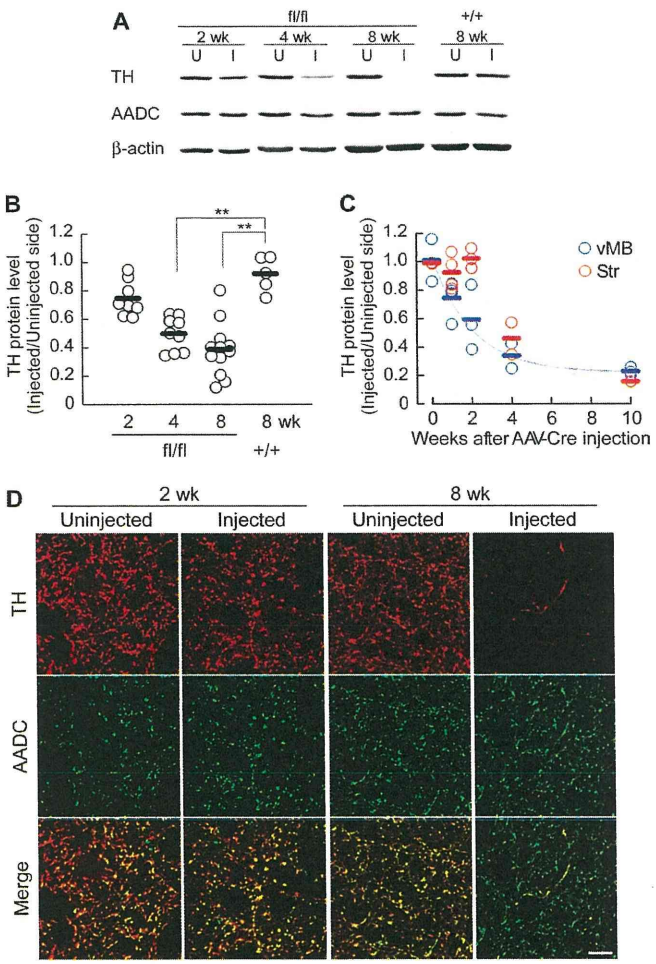

FIGURE 3. **Decrease in striatal TH protein levels after *Th* gene ablation.** *A*, striatal homogenates of each genotype were prepared 2, 4, or 8 weeks after the unilateral AAV-Cre injection into the SNc, and Western blot analysis was performed with antibodies against TH, AADC, and β-actin. *U* and *I*, uninjected and injected sides of the striatum, respectively. *B*, summarized quantitative analyses of Western blots for the striatal TH protein levels. The ratios of the protein level of the injected side to the uninjected side are plotted on the *vertical axis*. The *open circles* indicate the values from individual animals, and the *bars* indicate the means. $n = 8, 9, 12$, and 5 brains for 2, 4, and 8 weeks ($Th^{fl/fl}$ mice) and 8 weeks ($Th^{-/+}$ mice) after injection, respectively. *, $p < 0.05$; **, $p < 0.01$, Steel's test. *C*, comparison of TH protein levels in the striatum and ventral midbrain by Western blot. Tissue homogenates were prepared from the injected side and uninjected side of the ventral midbrain (*vMB*) and striatum (*Str*) of $Th^{fl/fl}$ mice and were subjected to Western blots for TH. $n = 2, 4, 3, 2$, and 3 for 0, 1, 2, 4, and 10 weeks after AAV-Cre injection, respectively. Data were fitted with an *exponential curve*. For the striatum, fitting was performed from 2 weeks because there was no apparent reduction before 2 weeks in this data set. *D*, decrease in the number of TH-expressing axons in the striatum. Striatal slices of the $Th^{fl/fl}$ mice were prepared 2 and 8 weeks after the injection of AAV-GFP/Cre and were immunohistochemically stained for TH (*red*) and AADC (*green*). TH and AADC were visualized as in Fig. 2*D*. *Merged images* are shown at the *bottom*. Images from the uninjected and injected side of the striatum are shown as indicated. *Scale bar*, 10 μm.

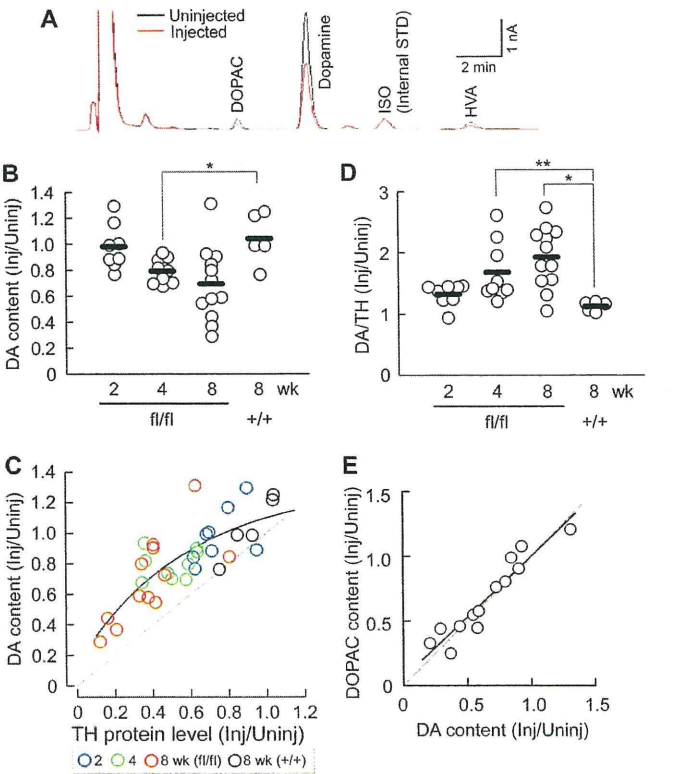

FIGURE 4. **The tissue dopamine contents are better maintained than TH protein levels in the striatum.** *A*, representative chromatograms of the monoamine assay with the homogenates from the uninjected and injected side striata from a $Th^{fl/fl}$ mouse 8 weeks after the injection of AAV-Cre. *B*, summarized DA contents in the striatum after the unilateral AAV-Cre injection to the SNc in the $Th^{fl/fl}$ and $Th^{+/+}$ mice. The monoamine assays were performed using the same extracts used in Fig. 3. The ratios of the dopamine contents in the injected side to the uninjected side are shown. The *open circles* indicate the values from individual animals, and the *bars* indicate the means. $n = 8, 9, 12$, and 5 brains for 2, 4, and 8 weeks ($Th^{fl/fl}$ mice) and 8 weeks ($Th^{+/+}$ mice) after the injection, respectively. *, $p < 0.05$, Steel's test. The mean dopamine contents in the uninjected side striata were 147.2 ± 10.2 and 158.1 ± 6.7 pmol/mg protein for $Th^{fl/fl}$ and $Th^{+/+}$ mice, respectively at 8 weeks (Steel's test, $p = 0.86$). *C*, the relationship between dopamine contents and TH protein levels. The *circles* represent data from individual animals and are *color-coded* by weeks after the AAV-Cre injection as indicated. The *dotted line* has a slope of 1. The *solid line* indicates an exponential curve fitting. The *points above* the *dotted line* suggest a higher dopamine level per TH protein level in the injected side compared with the uninjected side. *D*, ratio of the dopamine content to the TH protein level normalized to the uninjected side. $n = 8, 9, 12$, and 5 brains for 2, 4, and 8 weeks ($Th^{fl/fl}$ mice) and 8 weeks ($Th^{+/+}$ mice) after the injection, respectively. We excluded one outlier that showed very low TH protein levels and a high DA/TH ratio (29.8) from the 8-week $Th^{fl/fl}$ group. *, $p < 0.05$; **, $p < 0.01$, Steel's test. *E*, the relationship between DOPAC and dopamine contents in the $Th^{fl/fl}$ mice 8 weeks after the AAV-Cre injection. The data indicate the ratio of the DOPAC contents in the AAV-Cre-injected side of the striatum normalized to the uninjected side. The *open circles* indicate individual data. The *dotted line* has a slope of 1, and the *solid line* indicates a linear fitting. $n = 13$ mice. Spearman's rank correlation, $p < 0.0001$, $\rho = 0.96$ for DOPAC *versus* dopamine.

mice, respectively, compared with the $Th^{+/+}$ mice at 8 weeks; Fig. 4*B*). Notably, these reductions of dopamine contents were not as striking as those of TH protein levels (Fig. 2*C*). To evaluate the relationship between dopamine and TH, we plotted dopamine contents against TH protein levels (Fig. 4*C*). We found that dopamine contents were less affected than the TH protein levels, and the relationship was fitted well with an exponential curve ($\chi^2 = 0.7391$). The dopamine contents did not show a remarkable reduction until the TH protein levels were decreased by around 50%. Accordingly, the ratios of dopamine contents to TH protein levels were increased, with ratios of 1.32, 1.68, and 1.93 at 2, 4, and 8 weeks after the AAV-Cre injection, respectively, in the $Th^{fl/fl}$ mice, whereas it remained 1.1 in the $Th^{+/+}$ mice at 8 weeks (Steel's test, $p = 0.0665$, 0.0071, and 0.0157 for 2, 4, and 8 weeks for the $Th^{fl/fl}$ mice, respectively, compared with the $Th^{+/+}$ mice at 8 weeks; Fig. 4*D*).

Downloaded from www.jbc.org at JICHI IKA DAIGAKU, on February 27, 2012

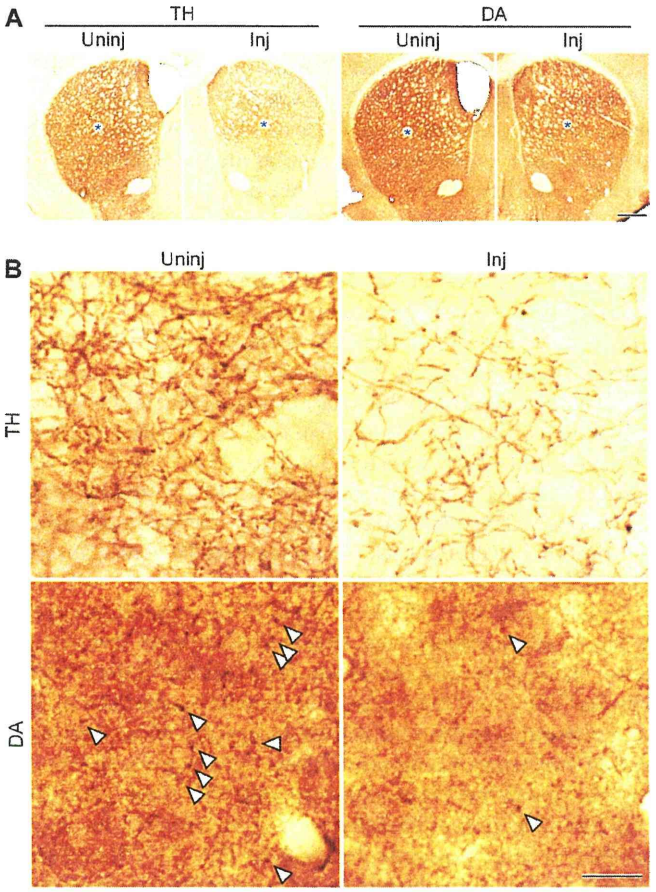

FIGURE 5. **TH and dopamine distribution in the striatum.** *A*, immunohistochemical detection of the striatal TH and DA in the striatum of the $Th^{fl/fl}$ mouse. The mice were fixed with glutaraldehyde 8 weeks after the injection of AAV-GFP/Cre, and the slices cut with a vibratome were stained with antibodies against TH or dopamine. Note that the TH signal in the injected side (*Inj*) was decreased compared with the uninjected side (*Uninj*), whereas the DA signal was less affected. *B*, magnification images of the regions indicated by *asterisks* in *A*, showing TH-expressing axon fibers and dopamine-containing axonal boutons. *Arrowheads* indicate representative puncta of the dopamine signals. *Scale bars*, 0.5 mm (*A*) and 10 μm (*B*).

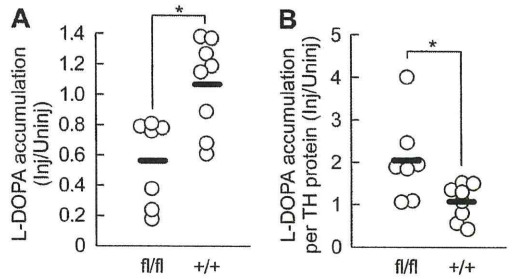

FIGURE 6. **Enhanced *in vivo* L-DOPA synthesis activity per TH protein level.** L-DOPA synthesis activities per TH protein level were estimated by measuring L-DOPA accumulation after *in vivo* administration of NSD-1015, an AADC inhibitor. Striatal homogenates were prepared 30 min after NSD-1015 administration (100 mg/kg, intraperitoneally). L-DOPA levels were measured by HPLC, and TH protein levels were assayed by Western blot. The mice were examined 8 weeks after the AAV-Cre injection. *A*, summary of L-DOPA accumulation in $Th^{fl/fl}$ and $Th^{+/+}$ mice. Data are shown as L-DOPA level in the injected side normalized by the uninjected side. The *open circles* indicate the values from individual animals, and the *bars* indicate the means. The mean L-DOPA level in the uninjected side of the $Th^{+/+}$ mice was 42.1 ± 7.3 pmol/mg protein. *B*, summary of L-DOPA accumulation normalized to the TH protein levels examined by Western blot, providing apparent L-DOPA synthesis activity per TH protein level. *, $p < 0.05$, Mann-Whitney *U* test.

It is known that unilateral depletion of dopamine in the rodent nigra induces ipsilateral rotation behavior in response to reagents enhancing dopaminergic transmission (25, 26). Consistently, $Th^{fl/fl}$ mice with severe unilateral dopamine depletion showed ipsilateral rotation behavior when administered with GBR12909, a potent DAT inhibitor (supplemental Fig. 2*B*), demonstrating the validity of our genetic manipulation to disrupt nigrostriatal dopaminergic transmission.

To further examine the tissue level alterations in the dopamine distribution, we used immunohistochemistry to determine the expression pattern for dopamine and TH in the striatum 8 weeks after the AAV-Cre injection. The mice were fixed transcardially with glutaraldehyde, and the striatal slices were stained with an antibody raised against dopamine-glutaraldehyde conjugate. We used immunoenzyme detection instead of immunofluorescence detection, because glutaraldehyde fixation causes a high fluorescence background. At a lower magnification, TH immunoreactivity was clearly reduced in the AAV-Cre-injected side of the $Th^{fl/fl}$ mice, whereas the dopamine immunoreactivity was only moderately reduced (Fig. 5*A*). These data are consistent with Western blot and monoamine assay results. Higher magnification views showed a reduction in the number of TH-expressing axon fibers in the AAV-Cre-injected side of the $Th^{fl/fl}$ mice (Fig. 5*B*) as observed by immunofluorescence staining (Fig. 3*D*). Moreover, the number of punctate signals of dopamine was also greatly decreased (Fig. 5*B*), suggesting that dopamine levels in the TH-lost axons were substantially reduced. Collectively, these data indicate a compensatory regulation of dopamine levels for a decrease in the TH protein levels. Because TH expression remained in only a subset of dopaminergic axons, these data raise the possibility that a decrease in dopamine synthesis induces a compensatory up-regulation of dopamine synthesis and/or storage in other axons.

Mechanisms of Dopamine Maintenance against TH Protein Loss—The homeostatic compensation of dopamine levels may accompany either an increase in the synthesis of dopamine or a decrease in the degradation of dopamine. To examine the degradation rate of dopamine, we measured the contents of 3,4-dihydroxyphenylacetic acid (DOPAC) and homovanillic acid (HVA), the two major metabolites of dopamine. Reductions of DOPAC and HVA contents were well correlated with that of dopamine in the $Th^{fl/fl}$ mice (Fig. 4*E*). Comparison between injected and uninjected sides showed no difference in the ratio of DOPAC to dopamine (DA) (injected side, 0.12 ± 0.02; uninjected side, 0.15 ± 0.03; Wilcoxon's signed rank test, $p = 0.16$) and in the ratio of HVA to dopamine (injected side, 0.13 ± 0.01; uninjected side, 0.14 ± 0.01; Wilcoxon's signed rank test, $p = 0.43$; supplemental Fig. 3). These data suggest that the degradation rate of dopamine was not significantly changed.

To explore a possible change in the activity of dopamine synthesis pathway, we evaluated *in vivo* L-DOPA synthesis activity by measuring L-DOPA accumulation 30 min after administration of NSD-1015, an AADC inhibitor, 8 weeks after the AAV-Cre injection. We found that the L-DOPA accumulation in the injected side of the striatum was significantly lower in the $Th^{fl/fl}$ mice compared with the $Th^{+/+}$ mice (Mann-Whitney *U* test, $p = 0.0206$; Fig. 6*A*). We then estimated the apparent L-DOPA

Downloaded from www.jbc.org at JICHI IKA DAIGAKU, on February 27, 2012

synthesis activity per TH protein by normalizing the L-DOPA accumulation with TH protein levels estimated by Western blot analysis. We found that the L-DOPA accumulation per TH protein in the injected side striatum was significantly higher in the $Th^{fl/fl}$ mice than in the $Th^{+/+}$ mice (Mann-Whitney *U* test, $p = 0.0279$; Fig. 6*B*). Considering that L-DOPA is mostly synthesized by TH (14), and the TH proteins remained to be expressed in only a subset of axons, these data suggest that dopamine synthesis activity in the remaining TH-positive axons was augmented to compensate for dopamine level.

Further, we examined if TH phosphorylation at Ser-31 and Ser-40 (27), the two major phosphorylation sites for TH activation, was elevated. However, we did not find a significant change in the phosphorylation states of these Ser residues by Western blot (supplemental Fig. 4). We also measured the contents of biopterin, an essential cofactor for TH, but the contents were not significantly different between the injected and uninjected side (uninjected side, 6.72 ± 0.54 pmol/mg protein; injected side, 6.64 ± 0.49 pmol/mg protein; Mann Whitney *U* test, $p = 0.95$). Thus, the long term up-regulation of L-DOPA synthesis activity may be supported by other molecular mechanisms (*e.g.* a relief of the feedback inhibition of TH by dopamine as a consequence of impaired dopamine synthesis).

In axon terminals, synthesized dopamine is primarily stored in synaptic vesicles, and released dopamine is partly recycled by DAT. When the number of TH-expressing axons was greatly reduced, the manner of dopamine storage could be changed for adaptation. In this context, we examined the level of two major dopamine transporters: vMAT2 and DAT. Western blot analysis showed no significant change in the vMAT2 and DAT protein levels in the injected side striatum compared with the uninjected side in the $Th^{fl/fl}$ mice, despite the great reduction of TH protein levels (supplemental Fig. 5). These data suggest that the numbers of dopaminergic synaptic vesicles and terminals were not grossly altered. Instead, because the majority of dopaminergic axons do not contain normal level of dopamine (Fig. 5*B*), despite the moderate decrease in tissue dopamine contents (Fig. 4), the vesicular dopamine contents in the TH-expressing axons may be increased, and/or TH-negative axons may uptake and contain low level dopamine.

DISCUSSION

Selective Loss of TH Protein in a Subset of Dopaminergic Neurons without Neuronal Degeneration—We took advantage of the Cre-*loxP* system in mice, which enabled us to selectively ablate the *Th* gene and block dopamine synthesis in adult brains. TH expression in the SNc was lost in a subset of SNc dopaminergic neurons by as early as 2 weeks after the AAV-Cre injection. The TH protein level and the number of TH-expressing axons in the striatum were clearly reduced 8 weeks after the AAV-Cre injection. Severe dopamine deficiency accompanied ipsilateral rotation behavior when stimulated with the DAT inhibitor, GBR12909, confirming the integrity of our genetic method to disrupt nigrostriatal dopaminergic transmission.

In contrast, the AADC protein levels and immunohistochemical signals in the striatum and SNc were unaffected 8 or 16 weeks after the AAV-Cre injection. These data suggest that the SNc dopaminergic neurons and axons were mostly preserved for several months without synthesizing dopamine. This is in contrast to neurodegenerative models using neurotoxins, such as 1-methyl-4-phenyl-1,2,3,6-tetrahydropyridine and 6-hydroxydopamine (6-OHDA), which could cause loss of axons and unpredictable side effects. Therefore, our experimental system provides a new animal model of chronic dopamine deficiency in adult brains without neuronal degeneration.

Differential Regulation of TH Protein Level in the Axon Terminals from Soma—Using this *Th* gene ablation strategy in adult brains, we noticed that the decline in the TH protein in the striatum was slower than the reduction of TH-expressing neurons in the SNc (Figs. 2*C* and 3*B*). By direct comparison of TH protein reduction in the striatum and ventral midbrain with Western blotting, we found that the TH protein reduction occurred in a delay, whereas the decay time constants were similar (Fig. 3*C*). This considerable delay of TH protein loss in the striatum suggests a mechanism that maintains the axonal TH protein level for a week or two without *Th* gene transcription. How does such a delay occur?

First, the turnover of TH proteins in axon terminals in the striatum may be slower than that in cell bodies in SNc. In cultured chromaffin cells, the steady-state half-life of the TH protein is about 1 day (28), but it could become longer than 10 days by treatment with translational inhibitors (29). Moreover, incubation with transcriptional inhibitors for 3 days caused no significant loss of the TH protein, although 90% of the TH mRNA was lost (29). Axonal translation may be involved for such a prolonged delay of protein degradation (30, 31). Thus, the difference in TH protein turnover in axon terminals and cell bodies located in SNc may be supported by those multiple regulatory mechanisms.

In addition, the delayed reduction of TH proteins may be attributable to slow axonal transport of TH proteins from soma to axons. Although the mechanism underlying axonal TH transport is not fully understood, the projection from SNc to the striatum in mice is about 2–10 mm, depending on axonal branching (22, 23). The axonal transport of TH was reported to be about 2 mm/h in chicken sciatic nerves (32), but it could be different in the brain because the cytosolic proteins are delivered by the slow axonal transport system at 0.1–8 mm/day (33, 34). These reports raise a possibility that it takes a week or more to transport TH proteins from a soma to axon terminals in the mouse nigrostriatal projection.

Regulation of Dopamine Levels by TH Protein Level and Activity in the Striatum—By quantitative comparison of dopamine contents with TH protein levels in the same striatal tissues, we found that dopamine contents were not simply determined by the TH protein level only. Notably, even 50% loss of TH protein did not remarkably change the dopamine contents. Eight weeks after the AAV-Cre injection, the TH protein levels were reduced to 39%, on average, whereas the dopamine contents were reduced to 69%. Immunohistochemical data showed a similar trend of difference. This finding is consistent with a previous report that dopamine contents in the brain of the adult $Th^{+/-}$ heterozygous mice are normally maintained despite a significant decrease in TH activity (12). Thus, these data indicate that the dopamine levels were primarily determined by TH

Downloaded from www.jbc.org at JICHI IKA DAIGAKU, on February 27, 2012

protein level but also influenced by another mechanism in the nigrostriatal projection.

In this study, we showed that (i) the TH protein expression was abrogated in a subset of dopaminergic neurons (AAV-Cre-infected neurons); (ii) the striatal dopamine contents were better maintained than the TH protein levels; and (iii) *in vivo* L-DOPA synthesis activity per TH protein level was enhanced. Because L-DOPA synthesis activity was virtually retained in only the TH-expressing axons, these results suggest that L-DOPA synthesis activity per TH protein in a given axon is partly affected by dopamine synthesis in the neighboring axons. Such trans-axonal regulation of dopamine synthesis activity might be a basis for the homeostasis of dopaminergic transmission in the striatum.

Consistent with our data, in a rat model of preclinical parkinsonism where nigrostriatal dopaminergic neurons were lesioned by 6-OHDA, TH activity was increased relative to dopamine loss (35). In such models generated with 6-OHDA, however, it is difficult to know if the enhanced TH activity observed after 6-OHDA administration is a result of a direct toxic effect of 6-OHDA on the remaining axons, a cell death of neighboring axons, or a decrease in tissue dopamine level. In contrast, our genetic manipulation specifically targets the *Th* gene in AAV-Cre-infected neurons, so our results demonstrate the effect of *Th* gene deletion on TH protein levels, dopamine contents, and L-DOPA synthesis activity more clearly and simply.

It remains to be determined how trans-axonal compensation of dopamine is mediated. For example, TH homospecific activity may be changed for the compensation by phosphorylation. D2 autoreceptors on dopaminergic axon terminals may be involved in controlling the dopamine level (36). However, it is not clear whether D2 autoreceptors modify dopamine synthesis in the long term. For example, chronic administration of haloperidol, a D2 receptor inhibitor, does not increase the basal levels of Ser(P)-31-TH and Ser(P)-40-TH in mice (37). We could not detect significant change in the Ser(P)-31-TH and Ser(P)-40-TH levels.

TH is also controlled by a feedback inhibition loop by dopamine (27). For example, a decrease in extracellular dopamine level by *Th* gene ablation may cause lower dopamine reuptake (38), lower local dopamine concentration in axon terminals, and a relief of TH from the feedback inhibition. Previous reports suggest that the concentration of released dopamine can be on the order of micromolar and is quickly taken up by DAT into dopaminergic axons (38). Because intracellular dopamine concentration is probably <100 nM (39), local intracellular dopamine concentration could be affected by dopamine reuptake. Meanwhile, TH has two dopamine-binding sites: high affinity (K_d < 4 nM) and low affinity (K_d = 90 nM) (40). Therefore, most TH proteins would be the dopamine-bound form for the high affinity site, whereas the low affinity site may be more relevant to feedback inhibition by dopamine (40).

Alternatively, there is a circuit level feedback (8) or neurotrophic factors, such as glial cell-derived neurotrophic factor (41). Further studies will be required to clarify the signaling mechanisms underlying the trans-axonal regulation of dopamine levels.

We found that the ratio of DOPAC and HVA contents to dopamine did not change, whereas, in Parkinson disease patients and model animals, DOPAC/DA and HVA/DA ratios were reported to be increased (7, 10, 42). This difference may exist because in our experimental conditions, most of the dopaminergic axons were preserved after the *Th* gene ablation, and those axons may have participated in the reuptake of extracellular dopamine, resulting in minimal effects on the dopamine degradation rate.

Adjusting Dopamine Storage for Compensation—If the number of dopamine-synthesizing axons was decreased by more than half, where and how were dopamine molecules stored for compensation? Because we did not observe any gross changes in the vMAT2 and DAT protein levels, it is unlikely that the numbers of dopaminergic synaptic vesicles and terminals were drastically changed. Otherwise, vesicular dopamine contents may be increased in the remaining TH-expressing axons for the compensation. For example, treatment of cultured dopaminergic neurons with L-DOPA or glial cell-derived neurotrophic factor increased vesicular dopamine levels more than 3-fold (41). Alternatively, it is also possible that the low level dopamine was contained in the TH-negative axons through the reuptake of spilled-over dopamine from neighboring synapses. This mechanism is consistent with the idea that released dopamine is spilled over and taken up by neighboring axons (38). Thus, the compensation of dopamine levels in our experimental system may accompany an increase in vesicular dopamine contents and/or spill-over and reuptake of released dopamine by TH-negative axons.

Taken together, in this study, we develop a conditional gene targeting method to efficiently and selectively inactivate the *Th* gene in the SNc dopaminergic neurons in adult mice without inducing neuronal degeneration. The analysis of these mutant mice revealed that TH protein levels in the axon terminals are regulated differently from the level in the soma, and the tissue dopamine levels are under trans-axonal compensatory regulation, where the reduction of dopamine in some axons induces up-regulation of dopamine synthesis activity in other axons. We believe that the present findings represent at least one of the compensatory mechanisms in Parkinson disease and are related to actions of remedies for psychiatric disorders.

Acknowledgments—We are most grateful to Professor Pierre Chambon for supporting this project. We thank Jean-Marc Bornert and the Institut de Génétique et de Biologie Moléculaire et Cellulaire/Institut Clinique de la Souris embryonic stem and mouse facility for excellent technical assistance. We thank Naomi Takino and Hiroko Nishida for technical assistance in constructing the AAV vectors. We thank Felix Schlegel for technical assistance with immunohistochemistry. We thank Dr. Pavel Osten for kindly providing the Synapsin I promoter construct.

REFERENCES

1. Graybiel, A. M., Canales, J. J., and Capper-Loup, C. (2000) *Trends Neurosci.* **23,** S71–S77
2. Schultz, W. (2007) *Trends Neurosci.* **30,** 203–210
3. Fahn, S. (2003) *Ann. N.Y. Acad. Sci.* **991,** 1–14
4. Grace, A. A., Floresco, S. B., Goto, Y., and Lodge, D. J. (2007) *Trends*

Downloaded from www.jbc.org at JICHI IKA DAIGAKU, on February 27, 2012

Neurosci. **30,** 220–227
5. Tye, K. M., Tye, L. D., Cone, J. J., Hekkelman, E. F., Janak, P. H., and Bonci, A. (2010) *Nat. Neurosci.* **13,** 475–481
6. Simpson, E. H., Kellendonk, C., Kandel, E. (2010) *Neuron* **65,** 585–596
7. Bernheimer, H., Birkmayer, W., Hornykiewicz, O., Jellinger, K., Seitelberger, F. (1973) *J. Neurol. Sci.* **20,** 415–455
8. Bezard, E., Gross, C. E., and Brotchie, J. M. (2003) *Trends Neurosci.* **26,** 215–221
9. McCallum, S. E., Parameswaran, N., Perez, X. A., Bao, S., McIntosh, J. M., Grady, S. R., and Quik, M. (2006) *J. Neurochem.* **96,** 960–972
10. Pifl, C., and Hornykiewicz, O. (2006) *Neurochem. Int.* **49,** 519–524
11. Perez, X. A., Parameswaran, N., Huang, L. Z., O'Leary, K. T., and Quik, M. (2008) *J. Neurochem.* **105,** 1861–1872
12. Kobayashi, K., Morita, S., Sawada, H., Mizuguchi, T., Yamada, K., Nagatsu, I., Hata, T., Watanabe, Y., Fujita, K., and Nagatsu, T. (1995) *J. Biol. Chem.* **270,** 27235–27243
13. Thomas, S. A., Matsumoto, A. M., and Palmiter, R. D. (1995) *Nature* **374,** 643–646
14. Zhou, Q. Y., Quaife, C. J., Palmiter, R. D. (1995) *Nature* **374,** 640–643
15. Zhou, Q. Y., and Palmiter, R. D. (1995) *Cell* **83,** 1197–1209
16. Szczypka, M. S., Kwok, K., Brot, M. D., Marck, B. T., Matsumoto, A. M., Donahue, B. A., and Palmiter, R. D. (2001) *Neuron* **30,** 819–828
17. Hnasko, T. S., Perez, F. A., Scouras, A. D., Stoll, E. A., Gale, S. D., Luquet, S., Phillips, P. E, Kremer, E. J., and Palmiter, R. D. (2006) *Proc. Natl. Acad. Sci. U.S.A.* **103,** 8858–8863
18. Nagatsu, T., Levitt, M., and Udenfriend, S. (1964) *J. Biol. Chem.* **239,** 2910–2917
19. Li, X. G., Okada, T., Kodera, M., Nara, Y., Takino, N., Muramatsu, C., Ikeguchi, K., Urano, F., Ichinose, H., Metzger, D., Chambon, P., Nakano, I., Ozawa, K., and Muramatsu, S. (2006) *Mol. Ther.* **13,** 160–166
20. Kadkhodaei, B., Ito, T., Joodmardi, E., Mattsson, B., Rouillard, C., Carta, M., Muramatsu, S., Sumi-Ichinose, C., Nomura, T., Metzger, D., Chambon, P., Lindqvist, E., Larsson, N. G., Olson, L., Björklund, A., Ichinose, H., and Perlmann, T. (2009) *J. Neurosci.* **16,** 15923–15932
21. Dittgen, T., Nimmerjahn, A., Komai, S., Licznerski, P., Waters, J., Margrie, T. W., Helmchen, F., Denk, W., Brecht, M., and Osten, P. (2004) *Proc. Natl. Acad. Sci. U.S.A.* **101,** 18206–18211
22. Paxinos, G., and Franklin, K. B. (2004) *The Mouse Brain in Stereotaxic Coordinates*, Academic Press, Inc., San Diego, CA
23. Prensa, L., and Parent, A. (2001) *J. Neurosci.* **21,** 7247–7260
24. Matsuda, W., Furuta, T., Nakamura, K. C., Hioki, H., Fujiyama, F., Arai, R., and Kaneko, T. (2009) *J. Neurosci.* **29,** 444–453
25. Ungerstedt, U., and Arbuthnott, G. W. (1970) *Brain Res.* **24,** 485–493
26. Lane, E. L., Cheetham, S., and Jenner, P. (2005) *J. Pharmacol. Exp. Ther.* **312,** 1124–1131
27. Dunkley, P. R., Bobrovskaya, L., Graham, M. E., von Nagy-Felsobuki, E. I., and Dickson, P. W. (2004) *J. Neurochem.* **91,** 1025–1043
28. Tank, A. W., Curella, P., and Ham, L. (1986) *Mol. Pharmacol.* **30,** 497–503
29. Fernández, E., and Craviso, G. L. (1999) *J. Neurochem.* **73,** 169–178
30. Lin, A. C., and Holt, C. E. (2008) *Curr. Opin. Neurobiol.* **18,** 60–68
31. Willis, D. E., and Twiss, J. L. (2006) *Curr. Opin. Neurobiol.* **16,** 111–118
32. Jarrott, B., and Geffen, L. B. (1972) *Proc. Natl. Acad. Sci. U.S.A.* **69,** 3440–3442
33. Terada, S. (2003) *Neurosci. Res.* **47,** 367–372
34. Hirokawa, N., Niwa, S., and Tanaka, Y. (2010) *Neuron* **68,** 610–638
35. Zigmond, M. J., Acheson, A. L., Stachowiak, M. K., and Stricker, E. M. (1984) *Arch. Neurol.* **41,** 856–861
36. Cubeddu, L. X., and Hoffmann, I. S. (1982) *J. Pharmacol. Exp. Ther.* **223,** 497–501
37. Håkansson, K., Pozzi, L., Usiello, A., Haycock, J., Borrelli, E., and Fisone, G. (2004) *Eur. J. Neurosci.* **20,** 1108–1112
38. Rice, M. E., and Cragg, S. J. (2008) *Brain Res. Rev.* **58,** 303–313
39. Mosharov, E. V., Larsen, K. E., Kanter, E., Phillips, K. A., Wilson, K., Schmitz, Y., Krantz, D. E., Kobayashi, K., Edwards, R. H., and Sulzer, D. (2009) *Neuron* **62,** 218–229
40. Gordon, S. L., Quinsey, N. S., Dunkley, P. R., and Dickson, P. W. (2008) *J. Neurochem.* **106,** 1614–1623
41. Pothos, E. N., Davila, V., and Sulzer, D. (1998) *J. Neurosci.* **18,** 4106–4118
42. Hefti, F., Enz, A., and Melamed, E. (1985) *Neuropharmacology* **24,** 19–23
43. Fukushima, T., and Nixon, J. C. (1980) Anal. Biochem. **102,** 176–188

Downloaded from www.jbc.org at JICHI IKA DAIGAKU, on February 27, 2012

Asari et al. BMC Neurology 2011, 11:35
http://www.biomedcentral.com/1471-2377/11/35

BMC Neurology

RESEARCH ARTICLE Open Access

Subregional 6-[^{18}F]fluoro-L-*m*-tyrosine Uptake in the Striatum in Parkinson's Disease

Sayaka Asari[1*], Ken-ichi Fujimoto[1], Akihiro Miyauchi[2], Toshihiko Sato[3], Imaharu Nakano[1] and Shin-ichi Muramatsu[1*]

Abstract

Background: In idiopathic Parkinson's disease (PD) the clinical features are heterogeneous and include different predominant symptoms. The aim of the present study was to determine the relationship between subregional aromatic l-amino acid decarboxylase (AADC) activity in the striatum and the cardinal motor symptoms of PD using high-resolution positron emission tomography (PET) with an AADC tracer, 6-[^{18}F]fluoro-L-*m*-tyrosine (FMT).

Methods: We assessed 101 patients with PD and 19 healthy volunteers. PD was diagnosed based on the UK Brain Bank criteria by two experts on movement disorders. Motor symptoms were measured with the Unified Parkinson's Disease Rating Scale (UPDRS). FMT uptake in the subregions of the striatum was analyzed using semi-automated software for region-of-interest demarcation on co-registered magnetic resonance images.

Results: In all PD patients, FMT uptake was decreased in the posterior putamen regardless of predominant motor symptoms and disease duration. Smaller uptake values were found in the putamen contralateral to the side with more affected limbs. The severity of bradykinesia, rigidity, and axial symptoms was correlated with the decrease of FMT uptake in the putamen, particularly in the anterior part. No significant correlation was observed between tremors and FMT uptake.

Conclusions: Decrease of FMT uptake in the posterior putamen appears to be most sensitive in mild PD and uptake in the anterior putamen may reflect the severity of main motor symptoms, except for tremor.

Background

Cardinal motor symptoms such as bradykinesia, rigidity, and tremor in Parkinson's Disease (PD) become apparent after a depletion of dopamine in the striatum to approximately 20% of normal levels and a reduction in aromatic L-amino acid decarboxylase (AADC) activity to 5%-20% of normal levels [1,2]. In PD, dopaminergic hypofunction in the striatum is not homogenous in association with the selective loss of ventral intermediate and lateral cell groups of the substantia nigra pars compacta that project to the posterior part of the striatum [3], although the reason for this selective vulnerability remains unknown.

Positron emission tomography (PET) is valuable for assessing altered dopamine function in PD. The first tracer used to visualize and assess the integrity of dopamine presynaptic systems was 6-[^{18}F]fluoro-L-dopa (FDOPA), a fluoro-analog of L-dopa [4]. FDOPA is taken up into the dopaminergic axon terminals and decarboxylated by AADC before being trapped and stored in synaptic vesicles. FDOPA uptake is highly correlated with viable dopaminergic cells in neurotoxin-lesioned monkeys [5] and in postmortem human PD brains [6]. A shortcoming complicating the use of this agent, however, is that metabolites of FDOPA (such as 3-*O*-methyl-[^{18}F]fluoro-L-dopa, which is formed by the action of the ubiquitous enzyme catechol-*O*-methyl-transferase (COMT)) enter the brain and diminish image contrast. An alternative agent is the non-catecholic tracer 6-[^{18}F] fluoro -L-*m*-tyrosine (FMT). FMT is also a good substrate for AADC but is not metabolized by COMT; thus, FMT uptake has approximately twice the sensitivity of FDOPA uptake and more fully represents the extent of AADC activity [7-10].

To elucidate the relationship between the main motor symptoms of PD and subregional AADC activity in the striatum, we applied a semi-automated segmentation method for extracting putaminal subregions from

* Correspondence: sasari@jichi.ac.jp; muramats@jichi.ac.jp
[1]Division of Neurology, Department of Medicine, Jichi Medical University, Tochigi, Japan
Full list of author information is available at the end of the article

BioMed Central

© 2011 Asari et al; licensee BioMed Central Ltd. This is an Open Access article distributed under the terms of the Creative Commons Attribution License (http://creativecommons.org/licenses/by/2.0), which permits unrestricted use, distribution, and reproduction in any medium, provided the original work is properly cited.

high-resolution FMT PET images that were co-registered with 3.0-tesla magnetic resonance (MR) images.

Methods

Subjects and clinical evaluation

Our sample consisted of 101 patients with PD and 19 healthy individuals. PD was diagnosed clinically according to the UK PD Society Brain Bank criteria [11]. All of the patients had bradykinesia and at least one of the three features of PD: 4-6 Hz resting tremor, rigidity, and postural instability. All of the patients had asymmetric onset and showed a positive response to dopaminergic medication. None exhibited atypical symptoms such as severe gaze palsy or symptomatic dysautonomia. The control group included healthy individuals with no history of neurologic or psychiatric diseases.

Motor symptoms were evaluated using the motor examination part of the Unified Parkinson's Disease Rating Scale (UPDRS). Motor subscores were determined as follows: tremor (motor UPDRS: 20 + 21), bradykinesia (motor UPDRS: 23 + 24 + 25 + 26), rigidity (motor UPDRS: 22), and axial (motor UPDRS: 18 + 19 + 27 + 28 + 29 + 30 + 31). The mini-mental state examination (MMSE) was used to assess cognitive function.

This study was approved by the Institutional Ethics Committee of Jichi Medical University and all participants gave written informed consent.

PET imaging

All patients stopped levodopa at least 16 h before PET. To increase the availability of the tracer, all subjects took 2.5 mg/kg of carbidopa (a peripheral AADC inhibitor) orally 1 h before FMT injection. Prior to the emission scan, a 10 min transmission scan was obtained for attenuation correction. Subsequently, 0.12 mCi/kg of FMT in saline was infused into an antecubital vein and a 30-90 min static three-dimensional acquisition was started simultaneously using a PET-CT (GEMINI GXL, Philips, Amsterdam, The Netherlands). Each subject also underwent 3.0-tesla MR imaging (Achieva 3.0 T, Philips) using an inversion recovery (IR) proton density (PD)-weighted pulse sequence to enhance the contrast of anatomical structures. The PET and MR imaging data were co-registered with a fusion processing program (Syntegra, Philips) to produce fusion images. This program provided manual and point-based image registration as well as automated methods of gray-value-based image registration, including a mutual information algorithm [12]. In addition, an adaptive level set of segmentation was used for coregistration of CT and MRI imaging data [13].

Semi-automated region of interest analysis

Regions-of-interest (ROIs) in the putamen and caudate nucleus were defined in three dimensions (3-D) bilaterally on the co-registered MR images where the striatum was best visualized. The putamen and the head of caudate nucleus were delineated by manual inspection on the three to five adjacent MR planes that corresponded to those planes on the PET images. The putamen was then automatically divided into three parts in the rostrocaudal direction using dedicated software for ROI demarcation. The 3-D ROIs (volumes of interest, VOIs) were extracted automatically by connecting two-dimensional drawings on each plane using a linear interpolation algorithm for VOI outlines. For reference, cerebellar ROIs were also defined in 3-D and located bilaterally on the cerebellar cortex.

Striatal-to-cerebellum ratio (SCR) values of radioactivity counts were calculated in the 80-90-min frame for each structure, using bilaterally averaged cerebellar ROI data as the denominator. For subregional analysis of their association with major motor symptoms in the PD subjects, SCR values from the caudate nucleus and each part of the putamen were analyzed on the contralateral to the more affected side of limb.

Statistical Analysis

For comparison of more than two groups, one-way analysis of variance (ANOVA) was used. When the one-way ANOVA was significant at $p < 0.05$, post-hoc comparisons were conducted using Scheffé's test. We examined the correlation of FMT uptake in each part of the putamen with disease duration, and with the symptoms of bradykinesia, tremor, rigidity, and postural instability assessed on UPDRS motor scores. Non-linear exponential regression analysis was applied to assess the relationship between FMT uptake and disease duration (Prism, GraphPad Software, La Jolla, CA). SCR values and the UPDRS scores were compared by Spearman's rank correlation coefficient test. $P < 0.05$ was considered to indicate a statistically significant difference.

Results

Characteristics of subjects

Demographic and clinical characteristics of the patients with PD and those of the control subjects are listed in Table 1 and Table 2. The mean ages of the PD patients (41 male and 60 female) and the control subjects (6 male and 13 female) were 64.0 years (SD 9.3) and 56.7

Table 1 Clinical Characteristics of the Subjects

Characteristics	PD	Normal Control	*p* value
Age, year, mean ± SD	64.0 ± 9.3	56.7 ± 11.1	0.005
Male/Female	41/60	6/13	0.542
MMSE	27 ± 2.6	29 ± 1.3	0.005

MMSE, Mini Mental State Examination.
Data are given as mean ± standard deviation (SD) values.

Table 2 Clinical Charasteristics of the PD patients

Symptom duration, year	6.0 ± 4.4
More affected side	Right 55/Left 46
Hoehn-Yahr stage, on	2.4 ± 0.9
Hoehn-Yahr stage, off	3.3 ± 1.1
UPDRS score	
Total motor	30.3 ± 16
Bradykinesia	9.86 ± 6.3
Rigidity	6.15 ± 3.8
Axial	9.54 ± 6.2
Tremor	4.80 ± 4.0

UPDRS, Unified Parkinson's Disease Rating Scale.
Data are given as mean ± standard deviation (SD) values.

years (SD 11.1), respectively. A wide range of duration and severity of symptoms was represented among the patients. The mean duration of symptoms was 6.0 years (SD 4.4) and the mean UPDRS motor score was 30.3 (SD 16.0). The right side was more affected in 55 patients.

Subregional analysis of FMT uptake

Figure 1 shows representative images of FMT uptake in a normal subject and in early- and late-stage PD patients. Among the patients, FMT uptake showed the most marked decrease in the posterior putamen, regardless of disease duration, but significant decrease was seen throughout the striatum compared with the healthy controls. There were significant differences between side (ipsi- vs. contralateral to the more affected limbs), region (anterior vs. posterior putamen), and diagnosis (healthy subjects vs. PD group) ($P < 0.001$) (Figure 2a). Asymmetry between the striatum of the more and less affected sides is preserved, but shows a decrease with disease progression (Figure 2b).

Decline in FMT uptake with disease duration

Figure 3 shows scatterplots of FMT uptake against symptom duration in three regions of the putamen contralateral to the more affected limbs. Because age-related factors such as age at onset of symptoms and age-related Alzheimer-type pathology may influence disease duration, we excluded elderly-onset patients (> 70 years old; $n = 19$) in this analysis. Exponential regression curves that best fitted the data for each of the three regions analyzed are superimposed on the figure. Between 10 and 15 years of symptom duration, the FMT for all three curves leveled off to constant values that showed a statistically significant difference between the anterior and posterior putamen ($p < 0.001$). In the control group, there was no significant difference in SCR of FMT uptake between younger (< 59 years old, $n = 10$) and older (≥ 60 years old, $n = 9$) subjects (putamen, $p = 0.87$; caudate, $p = 0.81$).

Correlation of cardinal symptoms and FMT uptake

To minimize the possibility of including patients with alternative diagnoses, we analyzed patients who had cardinal motor symptoms for at least 3 years ($n = 42$). We obtained positive correlations between the severities of major motor symptoms: rigidity vs. axial symptoms ($r = 0.68$, $p < 0.001$), rigidity vs. bradykinesia ($r = 0.56$, $p < 0.001$), bradykinesia vs. postural instability ($r = 0.54$, $p < 0.001$), and tremor vs. bradykinesia ($r = 0.39$, $p = 0.014$). However, tremor did not have a significant relation with rigidity ($r = 0.20$, $p = 0.20$) or with axial symptoms ($r =$

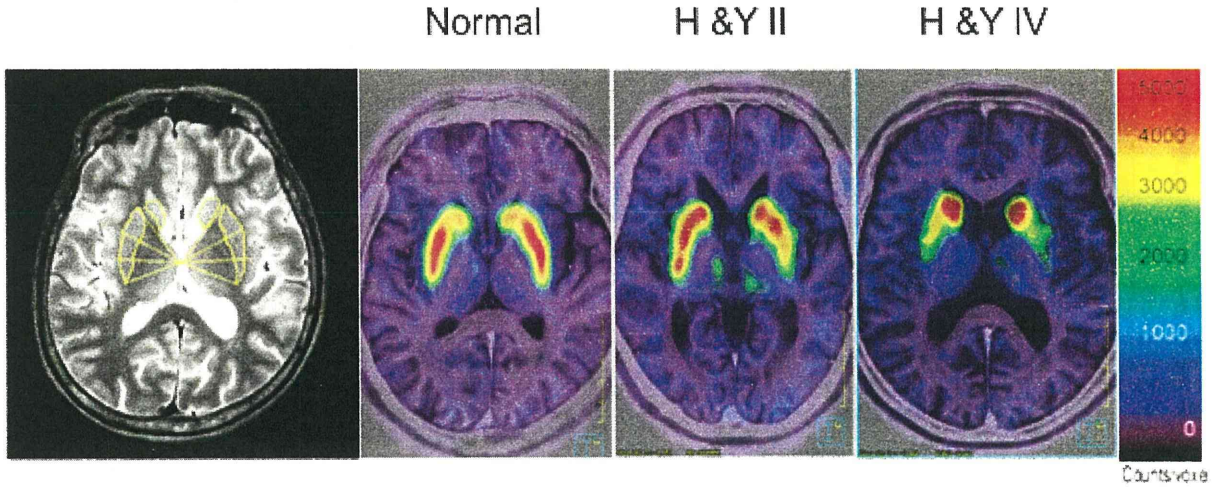

Figure 1 Representative FMT-PET images of a healthy individual and PD patients. FMT uptake declines asymmetrically in the early stages, mostly in the posterior putamen. Left: Regions-of-interest in the putamen. H &Y, Hohen and Yahr stage. The bar indicates the range of radioactive counts per voxel.

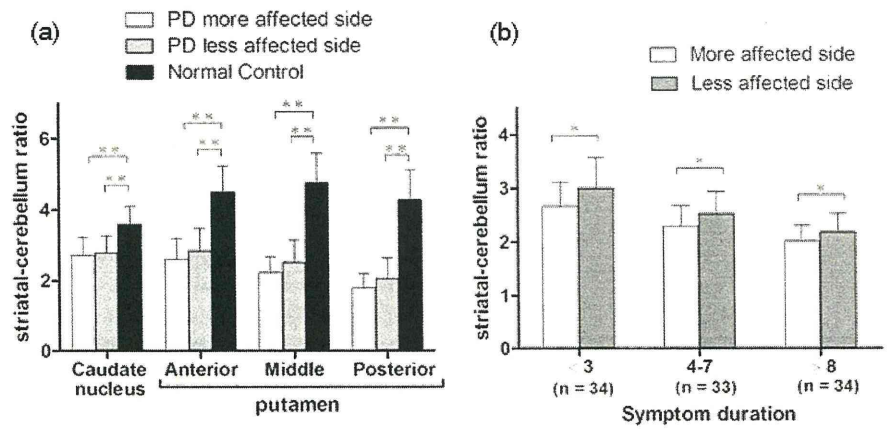

Figure 2 FMT uptake in different subregions of the striatum. Mean FMT uptake in different subregions of the striatum in normal control and PD patients (a). Comparison by side (b) shows persistant side-side asymmetry of putaminal uptake throughout the disease course. *$P < 0.05$, ** $P < 0.01$.

0.12, $p = 0.45$). Axial symptoms, rigidity, and bradykinesia scores showed a correlation with FMT uptake in the contralateral putamen, with the highest correlation in the anterior putamen, but not in the contralateral caudate (Table 3). No significant correlation was evident between unilateral tremor scores from the most severely affected limbs and any of the striatal regions. To assess the potential influence of age, we analyzed older patients (> 60 years old; $n = 25$) separately and found similar correlations between major symptoms and FMT uptake (Table 4).

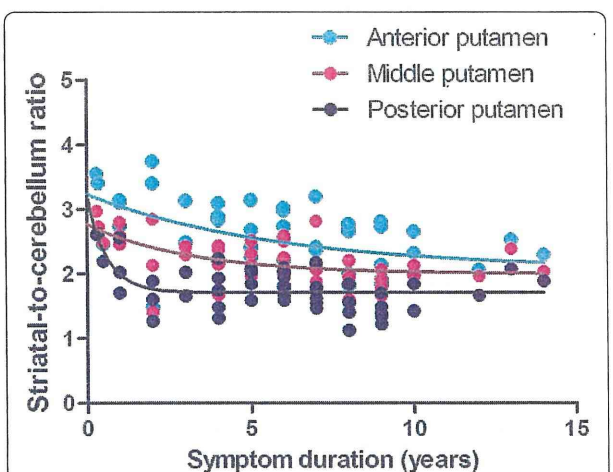

Figure 3 Decline in FMT uptake with disease duration. Scatter plots of FMT uptake against symptom duration in the putamen contralateral to the more affected limb in PD patients. Exponential decline is observed in all subregions of the putamen. Reduction of uptake is prominent at onset of the disease.

Discussion

Idiopathic PD is defined as a synucleinopathy in which Lewy bodies, pathological aggregations of the synaptic protein α-synuclein, are found in the dopaminergic neurons in the substantia nigra [14,15]. A reduction of dopamine in the striatum is a consistent finding in PD, although the clinical features are heterogeneous and include different predominant symptoms (resting tremor, bradykinesia, rigidity, or postural instability and gait disorder) with different rates of progression, and with or without dementia [16-19]. PET imaging is a valuable tool for assessing altered dopaminergic function in the striatum in PD. While FDOPA is suitable for assessing the metabolism of levodopa, FMT is superior for estimating AADC activity because it enables the production of higher-quality brain images [7,20-22]. The high resolution of FMT-PET images enables analysis of

Table 3 Correlations of UPDRS scores and FMT uptake ratio values in the each part of the putamen

Putamen	Anterior	Middle	Posterior	Whole
Symptom duration, year	-0.52 (<0.001)	-0.56 (<0.001)	-0.51 (<0.001)	-0.58 (<0.001)
Total motor score	-0.56 (<0.001)	-0.48 (0.002)	-0.41 (0.008)	-0.51 (0.001)
Bradykinesia	-0.54 (<0.001)	-0.53 (<0.001)	-0.44 (0.005)	-0.55 (<0.001)
Rigidity	-0.50 (0.001)	-0.43 (0.006)	-0.37 (0.018)	-0.44 (0.005)
Axial	-0.60 (<0.001)	-0.51 (0.001)	-0.37 (0.016)	-0.50 (0.001)
Tremor	0.069 (0.658)	0.085 (0.587)	0.015 (0.925)	0.050 (0.747)

Data are given as r (p) values. These values were calculated by Spearman's rank correlation coefficient test. UPDRS motor score in off-medication state was evaluated in 42 subjects.

Table 4 Correlations of UPDRS scores and FMT uptake ratio values in the each part of the putamen in elder patients

Putamen	Anterior	Middle	Posterior	Whole
Symptom duration, year	-0.70 (<0.001)	-0.63 (<0.005)	-0.45 (<0.05)	-0.70 (<0.001)
Total motor score	-0.56 (<0.01)	-0.50 (<0.05)	-0.37 (0.07)	-0.49 (<0.05)
Bradykinesia	-0.46 (<0.05)	-0.46 (<0.05)	-0.34(0.08)	-0.46 (<0.05)
Rigidity	-0.46 (<0.05)	-0.39 (0.05)	-0.31 (0.12)	-0.37 (0.06)
Axial	-0.69 (<0.001)	-0.59 (<0.01)	-0.45 (<0.05)	-0.58 (<0.01)
Tremor	0.26 (0.21)	0.12 (0.58)	0.06 (0.77)	0.14 (0.51)

Data are given as *r* (*p*) values. These values were calculated by Spearman's rank correlation coefficient test. UPDRS motor score in off-medication state was evaluated in 25 subjects.

dopaminergic presynaptic changes in each subregion of the striatum.

In the present study, FMT uptake in PD was reduced in the putamen, particularly in the posterior part. The anterior-to-posterior gradient of the uptake decrease in the putamen persisted to the advanced stage of PD. These results are consistent with those of previous reports that used other tracers of presynaptic dopaminergic terminals, and are considered to reflect the selective degeneration of nigrostriatal pathways that project into the posterior part of the putamen [23-25]. The lowest value of FMT uptake was observed in the posterior part of the putamen contralateral to the more affected limbs, even in the early stage of the disease. Because we analyzed regions in the posterior one-third of the putamen on high-resolution images, it is unlikely that the decreases in uptake were caused by partial volume effects, which may arise from placement of a small ROI on inaccurately co-registered images.

Post-mortem investigations of PD demonstrate that the rate of decrease of nigral neurons is rapid in the initial stage of the disease: approximately 40%-50% are lost in the first decade, possibly with a slower rate of degeneration later on, to finally approach a normal age-related linear decline [26]. In the present study, loss of FMT was well fitted to symptom duration using a single exponential approximation. The exponential model provided a better fit than a linear model, indicating that the rate of decline in FMT uptake in the contralateral putamen was faster at the beginning of the disease and slowed down as the disease progressed, in agreement with the results of previous studies that used radiotracers for imaging nigrostriatal nerve terminals [23-25]. Because we performed cross-sectional analysis in the present study, and because all of the participants were on medication, the data do not provide accurate information regarding the natural course of the disease, even if PET measurements were taken in off-medication state. Even so, the present data are important for assessing the progression of dopaminergic hypofunction in the striatum under optimal medical treatment, and can provide the basis for the development of even better therapeutic strategies [27,28].

We applied striatal count ratios to analyze the relationships between subregional putaminal FMT uptake and clinical symptoms. Striatal count ratios using the cerebellum as the denominator have a strong correlation with striatal uptake constants (Ki values) [29,30]. The present FMT-PET study showed a significant correlation between cardinal motor symptoms (rigidity, bradykinesia, and axial symptoms) and uptake of the tracer in the putamen, and no significant correlation was found between tremor score and FMT uptake. These findings are consistent with the results of previous PET studies [31-33]. The clinical correlations were more significant in the anterior part of the putamen than in the posterior part, possibly reflecting a floor effect for the uptake of FMT in the posterior part of the putamen, where the decrease was severe even in the early stage of the disease.

The pathophysiological mechanism of tremor is not fully understood [34]. Tremor does not respond to L-dopa as well as do bradykinesia and rigidity. The fact that stereotactic lesion or deep brain stimulation of the ventral intermediate nucleus (Vim) of the thalamus successfully improves tremor indicates a strong association between non-dopaminergic thalamic and cerebellar systems, and tremor generation [35,36].

Conclusions

Our results indicate that FMT-PET is useful for evaluating PD patients from the early stage of the disease and for studying the relationship between AADC activity and various clinical features. Decrease of FMT uptake in the posterior putamen appears to be most sensitive in mild PD, and uptake in the anterior putamen may reflect the severity of main motor symptoms, except for tremor. These data provide an important baseline for evaluating the effects of surgical interventions, such as gene therapy for PD.

Acknowledgements

This study was supported by grants from the Japanese Government: a Grant-in-Aid from the Research Committee of CNS Degenerative Diseases via the Ministry of Health, Labour and Welfare, and grants from the Ministry of Education, Culture, Sports, Science and Technology of Japan. The authors would like to thank Jun-ichi Saito and Seiji Nagashima for their technical assistance.

Author details

[1]Division of Neurology, Department of Medicine, Jichi Medical University, Tochigi, Japan. [2]WebNet Technology, Tochigi, Japan. [3]Utsunomiya Central Clinic, Tochigi, Japan.

Authors' contributions

SA participated in designing the study, data collection, conducted the statistical analyses, interpreted data and drafted the first manuscript.
KF participated in data collection and interpretation of data.
AM participated in data collection and interpretation of data.
TS participated in data collection and interpretation of data.
IN participated in designing the study and interpretation of data.
SM conceived the study, participated in its design, data collection, interpretation of data and drafting the manuscript.
All authors read and approved the final manuscript.

Competing interests

The authors declare that they have no competing interests.

Received: 6 October 2010 Accepted: 23 March 2011
Published: 23 March 2011

References

1. Hornykiewicz O: **Biochemical aspects of Parkinson's disease.** *Neurology* 1998, **51**:S2-9.
2. Nagatsu T, Ichinose H: **Molecular biology of catecholamine-related enzymes in relation to Parkinson's disease.** *Cell Mol Neurobiol* 1999, **19**:57-66.
3. Halliday G: **Substantia nigra and locus coeruleus.** In *The human nervous system.* 2 edition. Edited by: Paxinos G, Mai JK. Amsterdam; Boston: Elsevier Academic Press; 2004:pp457-458.
4. Garnett ES, Firnau G, Nahmias C: **Dopamine visualized in the basal ganglia of living man.** *Nature* 1983, **305**:137-138.
5. Pate BD, Kawamata T, Yamada T, McGeer EG, Hewitt KA, Snow BJ, Ruth TJ, Calne DB: **Correlation of striatal fluorodopa uptake in the MPTP monkey with dopaminergic indices.** *Ann Neurol* 1993, **34**:331-338.
6. Snow BJ, Tooyama I, McGeer EG, Yamada T, Calne DB, Takahashi H, Kimura H: **Human positron emission tomographic [^{18}F]fluorodopa studies correlate with dopamine cell counts and levels.** *Ann Neurol* 1993, **34**:324-330.
7. DeJesus OT, Flores LG, Murali D, Converse AK, Bartlett RM, Barnhart TE, Oakes TR, Nickles RJ: **Aromatic l-amino acid decarboxylase turnover in vivo in rhesus macaque striatum: a microPET study.** *Brain Res* 2005, **1054**:55-60.
8. DeJesus OT, Holden JE, Endres C, Murali D, Oakes TR, Shelton S, Uno H, Houser D, Freund L, Perlman SB, *et al*: **Visualization of dopamine nerve terminals by positron tomography using [^{18}F]fluoro-β-fluoromethylene-*m*-tyrosine.** *Brain Res* 1992, **597**:151-154.
9. Doudet DJ, Chan GL, Jivan S, DeJesus OT, McGeer EG, English C, Ruth TJ, Holden JE: **Evaluation of dopaminergic presynaptic integrity: 6-[^{18}F] fluoro-l-dopa versus 6-[^{18}F]fluoro-l-*m*-tyrosine.** *J Cereb Blood Flow Metab* 1999, **19**:278-287.
10. Eberling JL, Bankiewicz KS, O'Neil JP, Jagust WJ: **PET 6-[^{18}F]fluoro-l-*m*-tyrosine Studies of Dopaminergic Function in Human and Nonhuman Primates.** *Front Hum Neurosci* 2007, **1**:9.
11. Hughes AJ, Daniel SE, Lees AJ: **Improved accuracy of clinical diagnosis of Lewy body Parkinson's disease.** *Neurology* 2001, **57**:1497-1499.
12. Maes F, Collignon A, Vandermeulen D, Marchal G, Suetens P: **Multimodality image registration by maximization of mutual information.** *IEEE Trans Med Imaging* 1997, **16**:187-198.
13. Wells WM, Grimson WL, Kikinis R, Jolesz FA: **Adaptive segmentation of MRI data.** *IEEE Trans Med Imaging* 1996, **15**:429-442.
14. Dickson DW, Braak H, Duda JE, Duyckaerts C, Gasser T, Halliday GM, Hardy J, Leverenz JB, Del Tredici K, Wszolek ZK, Litvan I: **Neuropathological assessment of Parkinson's disease: refining the diagnostic criteria.** *Lancet Neurol* 2009, **8**:1150-1157.
15. Spillantini MG, Schmidt ML, Lee VM, Trojanowski JQ, Jakes R, Goedert M: **Alpha-synuclein in Lewy bodies.** *Nature* 1997, **388**:839-840.
16. Halliday GM, McCann H: **The progression of pathology in Parkinson's disease.** *Ann N Y Acad Sci* 2010, **1184**:188-195.
17. Maetzler W, Liepelt I, Berg D: **Progression of Parkinson's disease in the clinical phase: potential markers.** *Lancet Neurol* 2009, **8**:1158-1171.
18. Selikhova M, Williams DR, Kempster PA, Holton JL, Revesz T, Lees AJ: **A clinico-pathological study of subtypes in Parkinson's disease.** *Brain* 2009, **132**:2947-2957.
19. van Rooden SM, Heiser WJ, Kok JN, Verbaan D, van Hilten JJ, Marinus J: **The identification of Parkinson's disease subtypes using cluster analysis: a systematic review.** *Mov Disord* 2010, **25**:969-978.
20. Brown WD, DeJesus OT, Pyzalski RW, Malischke L, Roberts AD, Shelton SE, Uno H, Houser WD, Nickles RJ, Holden JE: **Localization of trapping of 6-[^{18}F]fluoro-l-*m*-tyrosine, an aromatic l-amino acid decarboxylase tracer for PET.** *Synapse* 1999, **34**:111-123.
21. DeJesus OT, Haaparanta M, Solin O, Nickles RJ: **6-fluoroDOPA metabolism in rat striatum: time course of extracellular metabolites.** *Brain Res* 2000, **877**:31-36.
22. Elsinga PH, Hatano K, Ishiwata K: **PET tracers for imaging of the dopaminergic system.** *Curr Med Chem* 2006, **13**:2139-2153.
23. Bruck A, Aalto S, Rauhala E, Bergman J, Marttila R, Rinne JO: **A follow-up study on 6-[^{18}F]fluoro-l-dopa uptake in early Parkinson's disease shows nonlinear progression in the putamen.** *Mov Disord* 2009, **24**:1009-1015.
24. Lee CS, Schulzer M, de la Fuente-Fernandez R, Mak E, Kuramoto L, Sossi V, Ruth TJ, Calne DB, Stoessl AJ: **Lack of regional selectivity during the progression of Parkinson disease: implications for pathogenesis.** *Arch Neurol* 2004, **61**:1920-1925.
25. Nandhagopal R, Kuramoto L, Schulzer M, Mak E, Cragg J, Lee CS, McKenzie J, McCormick S, Samii A, Troiano A, *et al*: **Longitudinal progression of sporadic Parkinson's disease: a multi-tracer positron emission tomography study.** *Brain* 2009, **132**:2970-2979.
26. Fearnley JM, Lees AJ: **Ageing and Parkinson's disease: substantia nigra regional selectivity.** *Brain* 1991, **114(Pt 5)**:2283-2301.
27. Christine CW, Starr PA, Larson PS, Eberling JL, Jagust WJ, Hawkins RA, VanBrocklin HF, Wright JF, Bankiewicz KS, Aminoff MJ: **Safety and tolerability of putaminal AADC gene therapy for Parkinson disease.** *Neurology* 2009, **73**:1662-1669.
28. Muramatsu SI, Fujimoto KI, Kato S, Mizukami H, Asari S, Ikeguchi K, Kawakami T, Urabe M, Kume A, Sato T, *et al*: **A Phase I study of aromatic l-amino acid decarboxylase gene therapy for Parkinson's disease.** *Mol Ther* 2010, **18**:1731-1735.
29. Dhawan V, Ma Y, Pillai V, Spetsieris P, Chaly T, Belakhlef A, Margouleff C, Eidelberg D: **Comparative analysis of striatal FDOPA uptake in Parkinson's disease: ratio method versus graphical approach.** *J Nucl Med* 2002, **43**:1324-1330.
30. Eberling JL, Pivirotto P, Bringas J, Bankiewicz KS: **Comparison of two methods for the analysis of [^{18}F]6-fluoro-l-*m*-tyrosine PET data.** *Neuroimage* 2004, **23**:358-363.
31. Martin WR, Wieler M, Stoessl AJ, Schulzer M: **Dihydrotetrabenazine positron emission tomography imaging in early, untreated Parkinson's disease.** *Ann Neurol* 2008, **63**:388-394.
32. Otsuka M, Ichiya Y, Kuwabara Y, Hosokawa S, Sasaki M, Yoshida T, Fukumura T, Masuda K, Kato M: **Differences in the reduced ^{18}F-Dopa uptakes of the caudate and the putamen in Parkinson's disease: correlations with the three main symptoms.** *J Neurol Sci* 1996, **136**:169-173.
33. Vingerhoets FJ, Schulzer M, Calne DB, Snow BJ: **Which clinical sign of Parkinson's disease best reflects the nigrostriatal lesion?** *Ann Neurol* 1997, **41**:58-64.
34. Rodriguez-Oroz MC, Jahanshahi M, Krack P, Litvan I, Macias R, Bezard E, Obeso JA: **Initial clinical manifestations of Parkinson's disease: features and pathophysiological mechanisms.** *Lancet Neurol* 2009, **8**:1128-1139.
35. Diamond A, Shahed J, Jankovic J: **The effects of subthalamic nucleus deep brain stimulation on parkinsonian tremor.** *J Neurol Sci* 2007, **260**:199-203.
36. Terao T, Yokochi F, Taniguchi M, Kawasaki T, Okiyama R, Hamada I, Nishikawa N, Izawa N, Shin M, Kumada S, Takahashi H: **Microelectrode findings and topographic reorganisation of kinaesthetic cells after gamma knife thalamotomy.** *Acta Neurochir (Wien)* 2008, **150**:823-827, discussion 827.

Pre-publication history

The pre-publication history for this paper can be accessed here:
http://www.biomedcentral.com/1471-2377/11/35/prepub

doi:10.1186/1471-2377-11-35
Cite this article as: Asari *et al.*: Subregional 6-[^{18}F]fluoro-L-*m*-tyrosine Uptake in the Striatum in Parkinson's Disease. *BMC Neurology* 2011 **11**:35.